

# Evaluation of high-resolution GRAMM/GRAL NO<sub>x</sub> simulations over the city of Zurich, Switzerland

Antoine Berchet<sup>1</sup>, Katrin Zink<sup>1</sup>, Dietmar Oettl<sup>2</sup>, Jürg Brunner<sup>3</sup>, Lukas Emmenegger<sup>1</sup> and Dominik Brunner<sup>1</sup>

<sup>1</sup>Empa, Swiss Federal Laboratories for Materials Science and Technology, Dübendorf, Switzerland.

<sup>2</sup>Air Quality Control, Government of Styria, Landhausgasse 7, 8010 Graz, Styria, Austria.

<sup>3</sup>Office for Environment and Health protection, City of Zürich, Zürich, Switzerland.

*Correspondence to:* A. Berchet (antoine.berchet@empa.ch)

## Abstract.

Hourly NO<sub>x</sub> concentrations were simulated for the city of Zurich, Switzerland, at 10 m resolution for the years 2013–2014. The simulations were generated with the nested mesoscale meteorology and microscale dispersion model system GRAMM/GRAL (versions v15.12/v14.8) by applying a catalogue-based approach. This approach was specifically designed to enable long-term city-wide building-resolving simulations with affordable computation costs. It relies on a discrete set of possible weather situations and corresponding steady-state flow and dispersion patterns that are pre-computed and then matched hourly with actual meteorological observations. The modelling system was comprehensively evaluated using eight sites continuously monitoring NO<sub>x</sub> concentrations and 65 passive samplers measuring NO<sub>2</sub> concentrations on a 2-weekly basis all over the city. The system was demonstrated to fulfil the European Commission standards for air pollution modelling at nearly all sites. The average spatial distribution was very well represented, despite a general tendency to overestimating the observed concentrations, possibly due to a crude representation of traffic-induced turbulence and to underestimated dispersion in the vicinity of buildings. The temporal variability of concentrations explained by varying emissions and weather situations was accurately reproduced on different time scales. The seasonal cycle of concentrations, mostly driven by stronger vertical dispersion in summer than in winter, was very well captured in the two year simulation period. Short-term events, such as episodes of particularly high and low concentrations, were detected in most cases by the system, although some unrealistic pollution peaks were occasionally generated, pointing at some limitations of the steady-state approximation. The different patterns of the diurnal cycle of concentrations observed in the city were generally well captured as well. The evaluation confirmed the adequacy of the catalogue-based approach in the context of city scale air pollution modelling. The ability to reproduce not only the spatial gradients but also the hourly temporal variability over multiple years makes the model system particularly suitable for investigating individualized air pollution exposure in the city.

## 1 Introduction

The urban population has grown steadily in the past century and already reached 50% globally and more than 75% in many developed countries. Urban areas with high population density are hot spots of air pollutant emissions, raising concerns regarding increased mortality and morbidity (Cohen et al., 2004; Jerrett et al., 2004; Beelen et al., 2013). Some of the most critical air pollutants in terms of health effects are particulate matter (PM) and NO<sub>2</sub>, whose levels exceed national and WHO standards in many urban areas (e.g., in Europe; Beelen et al., 2014). In Switzerland, and more particularly in urban centres such as the Zürich area, despite improving trends, the urban population is still exposed to harmful levels of PM smaller than 10  $\mu\text{m}$  (PM10) and NO<sub>2</sub> (Heldstab et al., 2011). Health effects of air pollution are well documented through numerous epidemiological studies (Brunekreef and Holgate, 2002; Beelen et al., 2008; Raaschou-Nielsen et al., 2013), but these studies rely on coarse estimates of the average population exposure as it is very challenging to account for the steep gradients and large temporal variability of air pollutant concentrations in cities (Jerrett et al., 2004; Beelen et al., 2008, 2013). Computing individualized pollution exposure in urban areas requires high-resolution simulations, with at least hourly resolution and spanning long periods of time (years to decades) since health impacts can be triggered by both short-term exceedances of pollution thresholds or long-term continuous exposure to high pollution levels (Van Roosbroeck et al., 2006; Beelen et al., 2008; Lelieveld et al., 2013). Individualized exposure is not only useful for epidemiological studies, but also for air quality plans designed by cities to reduce the direct and indirect social and economic costs of air pollution (e.g., Lelieveld et al., 2013). Current air quality plans are generally lacking a systematic cost-benefit assessment of different mitigation measures due to the lack of affordable model solutions that satisfy the demanding requirements in terms of resolution, temporal coverage, and source-specific information (Miranda et al., 2015).

In the present study, we focus on NO<sub>x</sub>, an air pollutant with particularly large spatial and temporal gradients due to its short lifetime (e.g., Vardoulakis et al., 2002). Representing the gradients in NO<sub>x</sub> concentrations in cities is not yet achievable by standard chemistry-transport models, as they are limited to horizontal resolutions of typically a few kilometres (e.g., Terrenoire et al., 2015). Recent progress in computational fluid dynamics (CFD) models makes it possible to run high-resolution dispersion simulations at the city scale (Li et al., 2006; Kumar et al., 2009, 2011; Di Sabatino et al., 2013). However, the prohibitive computational cost of these simulations prevents their application in the context of long-term urban exposure assessment (Parra et al., 2010). Currently, the most widely used models for urban exposure assessment and regulatory applications are models with a simplified parametrization of pollutant dispersion (e.g. Gaussian plume) such as ADMS (Stocker et al., 2012), AERMOD (Rood, 2014), SIRANE (Soulhac et al., 2011), IFDM (Lefebvre et al., 2011), or OSPM (Kakosimos et al., 2010). When correctly parametrized and calibrated, these models offer a reliable representation of the average concentration distribution in cities (Soulhac et al., 2011; Briant et al., 2013; Brandt et al., 2013). However, they have difficulties in representing the dispersion in

complex building and street canyon configurations and to properly reproduce the temporal (hourly) variability due to varying meteorology (e.g., Soulhac et al., 2012; Ottosen et al., 2015). With the growing availability of urban air pollution observations due to recent advances in (low-cost) sensor technology (Jiao et al., 2016; Gao et al., 2016), land-use regression models (LUR) are increasingly being used for air pollution assessment (Kumar et al., 2015b; Heimann et al., 2015), offering a performance comparable to CFD full physics models (Beelen et al., 2010). Yet, LUR models need a large amount of in-situ observations at strategic locations to represent the full spatial and temporal variability (Duvall et al., 2016; Mueller et al., 2015, 2016; Hasenfratz et al., 2015), and cannot be extended backward in time to satisfy the needs of long-term epidemiological studies.

Considering the respective strengths and limitations of the standard urban air pollution modelling systems, Berchet et al. (2017) proposed a novel method taking advantage of high resolution accurate CFD modelling while keeping computational costs affordable, by using a catalogue-based approach merged with routinely available meteorological observations. They showed that it was computationally feasible to simulate hourly concentration maps over multiple years at building-resolving resolution which successfully capture most of the variability in  $\text{NO}_x$  concentrations caused by variations in air flow and atmospheric stability. The main purpose of the present study is to provide a comprehensive evaluation of the above-mentioned method for  $\text{NO}_x$  concentrations in Zürich, Switzerland, for the years 2013–2014. The modelling domain covers the entire urban area of Zurich and includes 8 continuous  $\text{NO}_x$  monitoring sites as well as 65  $\text{NO}_2$  passive samplers. We demonstrate the high quality and robustness of the catalogue-based modelling system for hourly and daily concentrations. Furthermore, we identify sources of errors and uncertainties in the modelling system and propose additional steps to improve the methodology.

In Sect. 2, the modelling chain applied to generate time series of pollution maps is described. In Sect. 3, the set-up for the city of Zurich is presented including the available in-situ observations, the emission inventory, and auxiliary data sets. In Sect. 4, the performance of the model in terms of spatial distribution and temporal variability is evaluated with in-situ  $\text{NO}_x$  and  $\text{NO}_2$  measurements.

## 2 Approach and modelling system

### 2.1 Catalogue-based approach

Our approach relies on explicit physical simulations of air flow and pollutant dispersion. Such simulations on a city-wide domain must account for the cascade of scales influencing flow patterns, from the synoptic to the street and building scale. The synoptic scale defines the general meteorological conditions and the mean direction and strength of the large-scale flow in the city region. Land-use and topography restructure the synoptic weather at the regional scale by generating mesoscale phenomena such as thermally driven land-lake breezes and up- and down-slope circulations, urban heat islands, and channelling and blocking of the flow by the topography. Inside the city, these regional

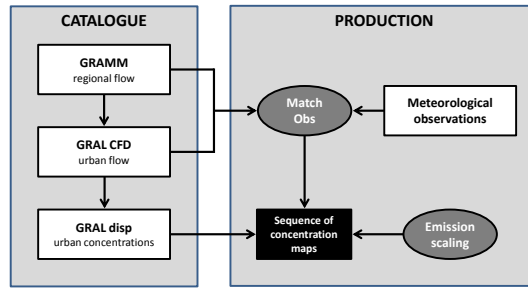


**Figure 1.** Scheme of the multi-step procedure to generate a sequence of hourly steady-state concentration maps from a catalogue of pre-computed wind and concentration fields. The dark grey ellipses are the method steps for generating time series of concentrations from the catalogue. Light grey rectangles denote intermediary products and inputs in the system.

conditions are further modified at the micro-scale by buildings and other obstacles such as vegeta-  
 tion. To properly account for this cascade of scales, our model approach is based on a three-step  
 100 procedure using the models GRAMM v15.12 (Graz meso-scale model; Almbauer et al., 2000) and  
 GRAL v14.8 (Graz Lagrangian model; Oettl, 2015b), further described in Sect. 2.2: i) mesoscale air  
 flow accounting for topography and land-use effects is computed by GRAMM for a larger domain  
 centered on the city, ii) microscale air flow inside the city, accounting for the effects of buildings  
 on flow and turbulence patterns, is inferred with the GRAL model, forced by GRAMM outputs, and  
 105 iii) Lagrangian dispersion computations are carried out by the dispersion module of GRAL, con-  
 strained by the micro-scale wind fields generated by GRAL. The GRAMM/GRAL system is briefly  
 described in Sect. 2.2.

Simulating the full transient evolution of the atmosphere over a multi-year period is not yet fea-  
 sible at building resolving resolution (i.e. better than 10 m) for a whole city with current computing  
 110 resources (e.g., Parra et al., 2010). Therefore, we approximate the full temporal dynamics by a se-  
 quence of steady-state solutions selected from a pre-computed catalogue as described in Berchet  
 et al. (2017). This catalogue is a discrete representation of all possible weather situations in terms of  
 atmospheric stability and of large-scale wind speed and direction at the boundaries of the domain.  
 Binning large-scale wind directions and speeds into 36 ( $10^\circ$  each) and 7 (from  $0.25$  to  $7 \text{ m}\cdot\text{s}^{-1}$ )  
 115 categories respectively, with seven possible Pasquill-Gifford classes for atmospheric stability as de-  
 fined by the U.S. Environment Protection Agency (2000) leads to a catalogue of 1008 physically  
 meaningful reference weather situations. As illustrated in Fig. 1, this catalogue is computed in a  
 three-step procedure which subsequently generates the mesoscale winds computed with GRAMM  
 and the corresponding urban-scale winds and air pollutant concentrations computed with GRAL.

120 Once the catalogue is available, a sequence of hourly weather situations is built based on in-situ  
 observations of wind speeds and directions in and around the city. For every hour of the simulated  
 period, the weather situation in the catalogue is selected whose associated wind field best matches

the in-situ observations. As demonstrated in Berchet et al. (2017), vertical stability and mesoscale flow patterns are intimately linked such that the stability can be sufficiently constrained by matching only the winds at a few selected locations in the model domain. The time series of hourly concentration distributions is then deduced directly from the sequence of weather situations. Generating concentration fields directly from matched weather situations and steady-state dispersion simulations implicitly attributes the influence of emissions at a specific time stamp entirely to the same hour, even though some virtual particles remain longer than one hour in the domain. It thus prevents accounting for the accumulation of air pollutants over subsequent hours and for flow changes during such periods of accumulation, but performs well in most cases as demonstrated in Sect. 4. Transport from remote sources outside of the simulation domain is represented by background concentrations as measured at a rural site near the city, and added to the simulated concentrations. This approach implicitly assumes that background concentrations are uniform over the whole modelling domain, even though small horizontal and vertical gradients may exist, especially in our set-up with complex topography. A future refinement of the approach would thus be desirable. To account for emissions varying independently from the weather, concentration maps in the catalogue are first computed using yearly average emissions and then scaled for each hour according to varying emission activity (e.g., diurnal cycle of traffic emissions). Since not all types of emissions follow the same temporal profile, emissions are divided into categories (see Sect. 3.3 and Tab. 1), for each of which a catalogue of concentration distributions is computed, and then scaled independently.

Thus, our catalogue-based method can be summarized by the following equation. At a given hour  $h$  and point  $\mathbf{x}$ , the simulated concentration can be written as:

$$c(\mathbf{x}, h) = c_{\text{background}}(h) + \sum_{i \in \text{sectors}} \tau_i(h) \times c_i(\eta(h), \mathbf{x}) \quad (1)$$

where  $\tau_i$  is the unitless temporal profile of emissions for each sector  $i$ ,  $c_{\text{background}}(h)$  the background concentrations measured at the distant site, and  $c_i(\eta(h), \mathbf{x})$  the simulated concentration field for sector  $i$  and weather situation  $\eta(h)$ , obtained with yearly average emissions. The weather situation  $\eta(h)$  best matching the meteorological observations at hour  $h$  is selected following Eq. 3 of Berchet et al. (2017).

Our modelling approach requires routinely available wind observations in the vicinity of the city of interest, and a background pollution observation site in the rural environment of the city. Berchet et al. (2017) concluded that 5–6 wind observation sites distributed around the city are generally sufficient to represent the variability of weather situations. The emission variability in Eq. 1 is determined from a wealth of information and models, including traffic counts (see Sect. 3) as proxies of emission variability. With such a catalogue-based approach, multi-year hourly physical simulations can be carried out at a cost of only 1–2 months of hourly simulations. The drawback of the approach

is that the full transient dynamics is replaced by a sequence of steady-state solutions, but as will be shown in this evaluation, this has only limited impact on the results.

## 2.2 GRAMM/GRAL modelling system

160 The catalogue-based approach relies on meteorological and on microscale flow and air pollutant dispersion simulations. The mesoscale simulations are carried out by GRAMM (Graz meso-scale model; Oetl, 2015a, 2016) and the microscale simulations by GRAL v14.8 (Graz Lagrangian model; Oetl, 2015b). GRAMM is a non-hydrostatic model solving the conservation equations for mass, enthalpy, momentum, and humidity. It accounts for contrasts in land use and corresponding  
165 surface fluxes of heat, momentum and humidity, and it has been specifically designed for operation in steep topography. The large scale weather conditions (wind speed and direction, stability class) of the catalogue are translated into parametrized vertical profiles of winds, temperature and pressure, as well as Obukhov length for different stability classes (following the Pasquill-Gifford classification: in the following, from A, very unstable situation, to G, extremely stable) to constrain the initial  
170 and boundary conditions of GRAMM simulations, as further detailed in Berchet et al. (2017), Oetl (2015a) and Oetl (2016).

GRAL is nested into GRAMM and is run here in diagnostic mode at 10 m resolution, which is different from Berchet et al. (2017) where GRAL was run in prognostic mode at 5 m resolution. In diagnostic mode, the flow field around buildings is computed by interpolating GRAMM wind  
175 fields on a fine Cartesian grid, and assuming a logarithmic wind profile close to walls. Finally, mass conservation is achieved by applying a Poisson equation to establish a pressure field to correct the velocities. In the prognostic mode, the flow is explicitly computed by forward integration of a set of prognostic equations. We chose here to use the diagnostic mode as the computation costs are lower, which allowed us to simulate a much larger domain covering the complete urban area of Zurich  
180 (see Sect. 3.1). We found only minor differences between the simulations with the two modes and resolutions and thus discuss only the results for the diagnostic mode in the following. Lagrangian dispersion simulations are computed with virtual particles released from prescribed emission sources (Oetl and Hausberger, 2006; Oetl, 2014) and transported according to the pre-computed GRAL wind fields. Turbulent diffusion is represented by specific Langevin equations applicable for the full  
185 range of wind speeds, in particular for low-wind-speeds (Anfossi et al., 2006).

## 2.3 Evaluation approach

The European Commission expert panel FAIRMODE (Forum for AIR quality MODelling in Europe) has been tasked to define quality objectives and performance criteria for air quality models, following the Directive 2008/50/EC of the European Parliament (EC, 2001). These criteria have been described  
190 in Thunis et al. (2012) and Pernigotti et al. (2013). They are based on the following metrics:

- normalized mean bias  $\text{NMB} = \frac{\bar{S} - \bar{O}}{\bar{O}}$ , with  $\bar{S}$  and  $\bar{O}$  the average simulations and observations, respectively;
- mean fractional bias  $\text{NFB} = \sum 2 \frac{s_i - o_i}{s_i + o_i}$ , with  $s_i$  and  $o_i$  individual simulated and observed values respectively,
- 195 – relative percentile error RPE, i.e., the relative error of the 90<sup>th</sup> percentile,
- FAC2, the fraction of simulations falling into a factor 2 of the observations,
- MQO, the model quality objective,  $\frac{\text{RMSE}}{2U}$ , with RMSE denoting the root mean square error and  $U$  the average model-observation uncertainty

The performance criteria specify thresholds for the above-mentioned metrics. They are either  
 200 defined as an absolute value (50% for RPE and FAC2; 1 for MQO) or are dependent on the model-observation uncertainty. As a pragmatic approach, the uncertainty  $U$  was chosen proportional to the observed and simulated values in Thunis et al. (2012). To adapt these definitions to urban simulations in the presence of very high concentration gradients, we add the range of simulated values within a 15-m radius around a given observation site to the uncertainties. Therefore, traffic sites with very  
 205 high local gradients have higher uncertainties than urban background sites. Scores are presented for two different simulated time series representing the concentrations at the exact location of the observation sites (reference), and the minimum of all concentrations in a radius of 15 m horizontally and 2 m vertically (minimum), respectively. The motivation for this will be presented in Sect. 4.1.

### 3 Setup for the city of Zurich

#### 210 3.1 Model domain

The model domain centered on the city of Zurich, Switzerland is illustrated in Fig. 2. The region is characterized by mountain ridges channelling the air flow and separating valleys where the population lives and where air pollution accumulates. In addition, the city of Zurich is located at the northern extremity of Lake Zurich, an elongated lake that covers an area of 120 km<sup>2</sup>, large enough  
 215 to generate weak land-lake breeze circulations. Mesoscale simulations with GRAMM are carried out in a domain spanning a region of 30 × 30 km<sup>2</sup>, with a horizontal resolution of 100 m. The simulation domain was chosen large enough to allow all topographic features potentially affecting the flow in the city to be represented. The domain extends vertically from the surface to 3000 m above ground with 22 geometrically spaced layers varying in thickness between 12 m close to the surface  
 220 and 500 m in the free troposphere.

Dispersion simulations are computed on a smaller domain embracing the whole city of Zurich and most of its outskirts, including some suburban agglomerations and industrial areas. GRAL is run at 10 m horizontal and 2 m vertical resolution on this 17 × 14 km<sup>2</sup>-large domain. Due to the

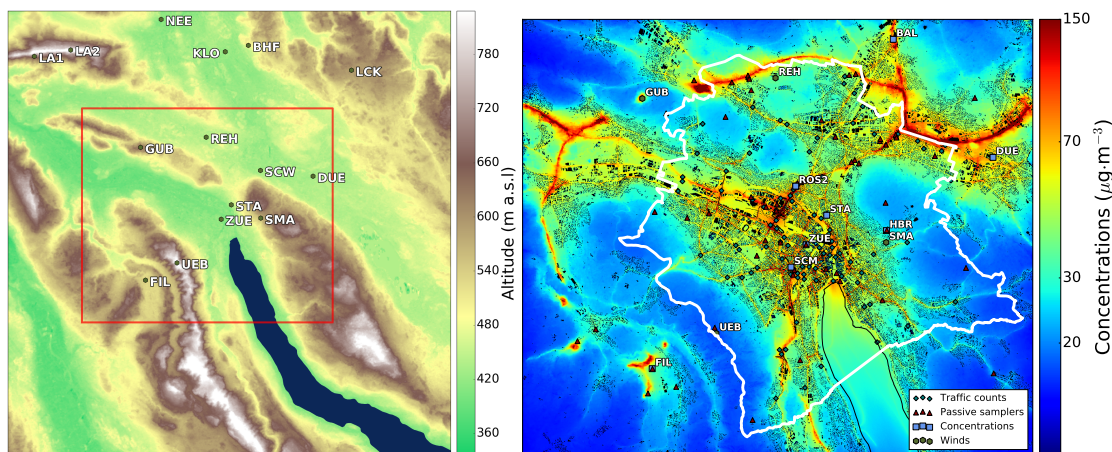


**Figure 2.** Simulation domains for the models GRAMM and GRAL. (left) GRAMM domain and wind measurement sites used in the match-to-observations procedure. The red rectangle is the domain covered by GRAL. (right) GRAL domain with in-situ observation sites overlaid on the 2013–2014 average  $\text{NO}_x$  concentrations as simulated by the modelling system. The political borders of the city are delimited by the white line.

hilly topography, highways are built through numerous tunnels, creating  $\text{NO}_x$  emission hotspots  
 225 at ventilation shafts and tunnel portals, which can optionally be treated in GRAL with a specific  
 algorithm described in Oettl et al. (2002), or simply as point sources at the tunnel gates.

### 3.2 General model inputs

As mentioned in Sect. 2, air flow computations require information on the topography, land-use  
 types and buildings. Topographical information was taken from the ASTER GDEM2 data set (Ad-  
 230 vanced Spaceborne Thermal Emission and Reflection Radiometer – Global Digital Elevation Map  
 Version 2) at a resolution of 30 m and projected to the 100 m GRAMM grid and linearly interpo-  
 lated to the 10 m GRAL grid. Information on land use (water bodies, forests, etc.) at a resolution  
 of 100 m was taken from the CORINE Land Cover data set (version CLC2006) distributed by the  
 European Environment Agency. The 44 CORINE land-use classes are translated into typical values  
 235 for roughness length, heat capacity and thermal conductivity, albedo and soil moisture for GRAMM  
 computations. GRAL uses land-uses classes in terms of roughness length to account for surface drag  
 caused by different types of vegetation, whereas the drag imposed by buildings is represented ex-  
 plicitly. The CORINE data set is projected similarly to ASTER to the GRAMM and GRAL grids.  
 Three-dimensional building information inside the city of Zurich was deduced from a vectorial build-  
 240 ing inventory provided by the municipality of Zurich. Buildings outside of the city are taken from  
 the nation-wide vectorial data base swissBUILDINGS3D v2.0, provided by the Swiss Federal Of-  
 fice of Topography, Swisstopo. Vectorial building shapes were projected to the 10 m GRAL grid, i.e.,  
 buildings are represented by individual blocks of  $10\text{ m} \times 10\text{ m}$  horizontal size.



Emission type	Simulated category	Inventory category	Resolution	Total emission $\text{t.y}^{-1} / \%$
Light duty traffic	UGZ light	Cars	7500 lines	495 / 18.0
		Motorbikes	7500 lines	5.7 / 2.7
	AWEL light	Cars	15500 lines	271.6 / 9.9
		Motorbikes	15500 lines	4.5 / 0.2
	AWEL area traffic	Non-road traffic	100 m grid	233.4 / 8.5
Heavy duty traffic	UGZ heavy	Heavy duty traffic	7500 lines	321.7 / 11.7
	UGZ bus	Buses	7500 lines	58.9 / 2.1
	AWEL heavy	Heavy goods vehicles	15500 lines	154.9 / 5.6
		Local delivery	15500 lines	77.8 / 2.8
	AWEL bus	Local buses	15500 lines	27.0 / 1.0
		Long-distance buses	15500 lines	13.8 / 0.5
Heating systems	UGZ heating	Oil boilers	10500 points	251 / 9.1
		Gas boilers	13200 points	138 / 5.0
	UGZ boilers	Hot-water generators	620 points	2.7 / 0.1
	UGZ wood	Wood-burning systems	900 points	18.7 / 0.7
	AWEL heating	Oil-gas systems	100 m grid	145.0 / 5.3
	AWEL wood	Wood-burning systems	100 m grid	26.6 / 1.0
Industry	UGZ industry	Medium-size industries	270 points	29.5 / 1.1
		Waste-burning and heat plants	56 points	175 / 6.3
	UGZ off-road	Construction machines	vector areas	75.5 / 2.8
	AWEL industry	Medium and large industries	100 m grid	86.3 / 3.1
		Industrial vehicles	100 m grid	100.8 / 3.7
		Smaller industrial emissions	100 m grid	4.8 / 0.2
Ships	UGZ ships	lake-cruise boats	cruise lines	20.9 / 0.8
	UGZ private boats	privately-owned boats	lake area	5.6 / 0.2
Total				2744.4 / 100

**Table 1.** Description of  $\text{NO}_x$  emission inventories in Zurich as used in GRAL simulations. Emissions inside the limits of the city of Zurich are provided by UGZ, emissions for the rest of the domain by AWEL.

### 3.3 Emission data

245 Emission data are deduced from two very detailed inventories produced by the municipal (Umwelt-  
und Gesundheitsschutz, UGZ) and cantonal (Amt für Abfall, Wasser, Energie und Luft, AWEL)  
environment authorities. Inventory information are detailed in Tab. 1. Both inventories are spatially  
explicit bottom-up inventories based on activity data and emission factors as detailed in e.g., FOEN  
(2010) and Heldstab et al. (2016). The two inventories have been designed for the year 2010 and  
250 are highly consistent in terms of total emissions over the domain of Zurich.  $\text{NO}_x$  emissions at the  
national scale are reported to have decreased by 5–10% depending on the emission category between  
2010 and the period of our simulations. We assume that city emissions follow the national trend and  
apply corresponding correction factors separately to the individual emission categories.

The UGZ inventory details emissions from thousands of individual sources as line, point or area  
255 sources divided into 60 emission categories (cars, motorbikes, gas heating systems, wood heating  
systems, etc.) within the city limits. Although accounted for in the UGZ inventory, some of these  
emission categories have a very marginal contribution to the  $\text{NO}_x$  emissions (e.g., forestry and agri-  
culture machines, smokers, animals), or are very punctual (e.g., fireworks), and have therefore been  
ignored in our simulations. These neglected emissions account for less than 1% of total  $\text{NO}_x$  emis-  
260 sions. Individual heating systems are registered by type and size and by the exact location and ele-  
vation of the chimney and treated as 26000 individual point sources. Emissions from cars, motorcy-  
cles, lorries and buses are represented as line sources segmented into 5 to 50 m-long segments and  
are based on a comprehensive traffic-emission model and manual traffic-counting campaigns; tun-  
nel portal are modelled as point sources integrating traffic emissions inside the tunnel. The AWEL  
265 inventory is less detailed but covers areas that are outside of the city but still inside the GRAL do-  
main. It describes 20 different emission categories as line or area sources. Main roads are described  
as line sources, while other sources are represented as area sources with a 100 m resolution grid.  
AWEL emissions are disaggregated to the GRAL grid using the building mask to attribute heating  
and industrial emissions to building roofs and other emissions to the space between buildings.

270 As GRAL can account for the rise of hot plumes in ambient air by applying a slightly modified  
version of the plume-rise model described in Hurley et al. (2005), an initial exhaust temperature and  
speed is prescribed for point emissions. Such values are available only for the biggest emitters such  
as waste incineration plants. For all other heating systems, a standard temperature and exhaust speed  
of 70° C and 0.8 m·s<sup>-1</sup> with a stack diameter of 0.5 m was prescribed. To account for the turbulence  
275 induced by the traffic at least to first order, emissions from car and heavy duty traffic are initially  
mixed within a volume defined by the width of the street (uniformly set at 7 m) and a height of 3 m  
above street level.

To limit the computational demand, we merged the original categories into a total of 25 group-  
categories by adding up emissions with a similar temporal profile. For instance, we expect motor-  
280 bike emissions to vary similarly to car emissions. Emission variability in Eq. 1 is determined based

on both pre-defined profiles and measured proxies. For all computed emission categories, we apply typical diurnal, weekly and seasonal cycles as used in the TNO-MACC emission inventory for Europe (Kuenen et al., 2011), with the exception of light duty traffic and heating emissions. 85 traffic counts are operated by the municipality in the city of Zurich. We use the hourly ratios of the total number of vehicles (summed over all sites) to the annual average hourly total. Heating emissions follow a diurnal cycle as prescribed in the TNO-MACC emission inventory, but the seasonal cycle of such emissions is determined using so-called “heating-degree days” accounting for the outdoor temperatures as measured at different locations in the city. Heating degree days are computed at the daily scale using Eq. 2:

$$\begin{aligned}
 \text{HDD}(t) &= T_{\text{ref}} - T(t) && \text{if } T(t) < T_{\text{min}} \\
 &= 0 && \text{else}
 \end{aligned}
 \tag{2}$$

with  $T_{\text{ref}} = 20^\circ\text{C}$  and  $T_{\text{min}} = 16^\circ\text{C}$  and  $T(t)$  the daily average outdoor temperature in the city at time  $t$ .

Heating emissions are scaled proportionally to the heating degree days parameter. As the total number of heating degree days varies from one year to another, depending on the meteorology, the scaling factor for heating emissions is chosen to keep consistent heating degree days and emissions for the year 2010 for which the inventory was designed.

### 3.4 Meteorological and air pollution observations

Meteorological observation sites used for the match-to-observations procedure are shown on the GRAMM domain of Fig. 2. Wherever possible, weather observations are compared with GRAL wind simulations as they are able to represent the influence of nearby obstacles on the air flow. Outside of the GRAL domain, GRAMM mesoscale simulations are used, which limits the selection to standard weather observation sites in open terrain following WMO recommendations as operated by the Swiss Federal Office of Meteorology and Climatology, MeteoSwiss. The remaining weather observations are obtained from air pollution observation sites, maintained by the Swiss national air pollution monitoring network, NABEL, the regional monitoring network for East-Switzerland, OSTLUFT, and the city environment authority, UGZ. At all MeteoSwiss sites but UEB and LA2, wind speeds and directions are measured on top of a 10-m tall meteorological mast. At UEB and LA2, wind measurements are carried out on top of a 189 m- and 32 m high telecommunication tower, respectively. Weather observation sites within the city are located above building roofs or in street canyons.

Eight  $\text{NO}_x$  concentration measurement sites used for evaluating the model are operated within the GRAL domain. GRAL concentrations in the corresponding cells are used for the assessment of the model performance. The rural site TAE, operated by NABEL 25 km away from the GRAL domain boundaries, is taken as regional background site. The site ZUE is located in the centre of

315 Zurich in a courtyard, distant from emission hot spots. The sites BAL, ROS, STA and SCM are  
located next to busy streets. DUE is operated in the outskirts of the city in a mixed industrial and  
residential area. HBR is located on the Zurichberg mountain, 200 m above the city centre level, at  
the limit of the built-up area next to a forest. At all sites, the air inlet is located at 3–4 m above  
ground level. NO<sub>x</sub> concentrations are measured with standard NO<sub>x</sub> monitors: Horiba APNA 360 and  
320 Horiba APNA 370. The Horiba APNA instruments use molybdenum converters to convert NO<sub>2</sub> into  
NO before measuring NO by chemiluminescence. These instruments are therefore also sensitive to  
other reactive nitrogen compounds, which may lead to some bias in the NO<sub>2</sub> measurements during  
periods when NO<sub>2</sub> concentrations are low but the concentrations of ozone and other photo-oxidants  
high (Steinbacher et al., 2007). Such bias are expected to impact significantly the background site  
325 TAE as discussed in Sect. 4.2. The instruments are automatically calibrated every 25 h and manually  
every 2 weeks at NABEL sites, and every 10 days at UGZ and OSTLUFT sites. The calibration is  
carried out through dynamic dilution of a certified NO mixture (Carbagas).

All the sites mentioned above provide continuous hourly measurements for the simulated period  
from January 2013 to December 2014. The monitoring network is complemented by a network of  
330 65 passive NO<sub>2</sub>-samplers maintained by UGZ and OSTLUFT. These samplers are collected every  
2 weeks and analysed in the laboratory shortly after collection. For making the biweekly samples  
comparable to the continuous observations, a few passive samplers are placed next to continuous  
sites. NO<sub>2</sub> observations from all passive samplers are then corrected with a linear correction function  
by comparing continuous and passive measurements at these sites.

335 Temperature data used to scale emissions from heating systems is gathered at the same locations  
as the wind data. The average outdoor temperature for the entire city is calculated as the mean of  
available observations. Traffic counts are located all around the city. They count vehicles indifferent  
of their type on a 15-minute-basis direction-wise for all lanes of selected streets. We use hourly totals  
in the city to scale traffic emissions uniformly.

## 340 **4 Results**

After generating the catalogue of wind and concentration fields, hourly time series of concentration  
maps have been generated for the years 2013 and 2014. In the following, these model outputs are  
evaluated against observations and an analysis of uncertainties of the model system is presented.

### **4.1 General model performance**

345 Our model is evaluated at all sites against the FAIRMODE performance criteria as defined in Sect. 2.3.  
All FAIRMODE scores are reported in Tab. 2. In the reference simulation, most sites fulfil the crite-  
ria. No more than ~ 15% of all computed scores are beyond the FAIRMODE performance criteria.  
The few exceptions are discussed below.

Temporal scale	Simulation ID	Site ID	Observed mean ( $\mu\text{g}\cdot\text{m}^{-3}$ )	15-m radius range ( $\mu\text{g}\cdot\text{m}^{-3}$ )	NMB (%)		MFB (%)		RPE (%)		FAC2 (%)		$r$		MQO
Hourly	Ref	HBR	23.1	7.1	46	29	46	30	50	27	50	78	0.66	0.78	0.81
		FIL	38.1	6.6	37	36	37	29	50	36	50	64	0.78	<b>0.61</b>	<b>1.37</b>
		DUE	45.1	10.3	43	40	43	43	50	33	50	61	0.78	<b>0.62</b>	<b>1.31</b>
		ZUE	46.6	12.9	42	26	42	28	50	23	50	76	0.68	0.73	0.93
		STA	63.9	30.3	53	29	53	33	50	23	50	73	0.46	0.75	0.68
		BAL	93.5	70.8	77	25	77	9	50	35	50	66	0.0	0.53	0.68
		SCM	95.9	58.7	65	52	65	36	50	<b>62</b>	50	68	0.27	0.66	0.80
		ROS	119.8	331.2	69	<b>135</b>	69	67	50	<b>165</b>	50	<b>43</b>	0.23	0.62	<b>1.07</b>
		ROS2	119.8	322.7	69	<b>79</b>	69	45	50	<b>102</b>	50	56	0.0	0.60	0.79
		All	65.3	57.3	106	51	106	33	50	<b>52</b>	50	67	0.0	0.67	0.66
Hourly	Min	HBR	23.1	7.1	46	8	46	14	50	8	50	85	0.66	0.79	0.78
		FIL	38.1	6.6	37	18	37	18	50	17	50	68	0.78	<b>0.64</b>	<b>1.25</b>
		DUE	45.1	10.3	43	22	43	31	50	15	50	66	0.78	<b>0.64</b>	<b>1.23</b>
		ZUE	46.6	12.9	42	-8	42	5	50	-15	50	83	0.68	0.76	0.92
		STA	63.9	30.3	53	-11	53	1	50	-17	50	83	0.46	0.79	0.63
		BAL	93.5	70.8	77	-6	77	-13	50	3	50	62	0.0	0.58	0.53
		SCM	95.9	58.7	65	-4	65	-1	50	-2	50	81	0.27	0.72	0.52
		ROS	119.8	331.2	69	17	69	9	50	31	50	70	0.23	0.58	0.52
		ROS2	119.8	322.7	69	18	69	10	50	32	50	70	0.0	0.58	0.53
		All	65.3	57.3	106	1	106	7	50	-1	50	76	0.0	0.71	0.38
	Ref	HBR	23.1	7.0	39	28	39	32	50	19	50	92	0.60	0.93	0.41
		FIL	36.0	6.1	31	<b>33</b>	31	31	50	37	50	80	0.73	0.83	0.79
		DUE	44.6	10.2	36	<b>40</b>	36	43	50	25	50	72	0.70	0.85	0.71
		ZUE	46.7	13.0	37	26	37	30	50	21	50	90	0.60	0.87	0.58
		STA	64.0	30.4	46	29	46	32	50	20	50	87	0.20	0.87	0.41
		BAL	93.3	69.8	52	24	52	13	50	39	50	86	0.0	0.70	0.52
		SCM	96.0	58.9	56	52	56	39	50	<b>60</b>	50	78	0.0	0.81	0.47
		ROS	119.8	331.7	48	<b>135</b>	48	<b>78</b>	50	<b>151</b>	50	<b>31</b>	0.07	0.75	0.78
		All	64.6	56.0	85	51	85	36	50	<b>63</b>	50	79	0.0	0.80	0.54
		Daily	Min	HBR	23.1	7.0	39	7	39	14	50	1	50	98	0.60
FIL	36.0			6.1	31	15	31	17	50	18	50	88	0.73	0.84	0.76
DUE	44.6			10.2	36	22	36	31	50	8	50	84	0.70	0.86	0.72
ZUE	46.7			13.0	37	-7	37	2	50	-15	50	98	0.60	0.88	0.69
STA	64.0			30.4	46	-11	46	-4	50	-18	50	98	0.2	0.89	0.45
BAL	93.3			69.8	52	-7	52	-13	50	5	50	88	0.0	0.73	0.39
SCM	96.0			58.9	56	-4	56	-3	50	-2	50	97	0.0	0.84	0.33
ROS	119.8			331.7	48	17	48	17	50	14	50	97	0.07	0.74	0.34
All	64.6			56.0	85	1	85	6	50	2	50	94	0.0	0.86	0.26

**Table 2.** Model performance for  $\text{NO}_x$  concentrations at all observation sites at the hourly and daily scales. Ref = standard simulation at the exact location of observation sites; Min = simulated minimum in a radius of 15 m horizontally and 2 m vertically. The score metrics are defined in Sect. 2.3. The left column for each score represents the FAIRMODE performance objective (defined in Sect. 2.3) following Thunis et al. (2012) dependent on  $U$ ; the right column is the computed score. Values not fulfilling the FAIRMODE objective are reported in bold. Sites are sorted by increasing observed mean.

At the site ROS, the model largely overestimates the concentrations, resulting in poor scores for  
350 NMB, FAC2, RPE and MQO. This can be explained by the very steep gradients in the vicinity of  
the site. ROS is located on a small parking lot, adjacent to the busiest traffic corridor in the city.  
Simulated concentrations vary spatially by more than  $300 \mu\text{g}\cdot\text{m}^{-3}$  within a radius of 15 m around  
the exact location of the site, compared to the observed average of  $120 \mu\text{g}\cdot\text{m}^{-3}$ . Small errors in  
the location of the emissions relative to the site or in the computation of the flow fields have a  
355 critical impact on such a site. At the site SCM, the relative percentile error exceeds the requirement  
threshold due to overestimated concentration peaks. The site SCM is a traffic site similar to ROS,  
with likely similar reasons for overestimation. However, an overestimation at SCM is only evident  
for the highest concentrations whereas at ROS the concentrations are generally too high. The sites  
FIL and DUE do not fulfil all FAIRMODE performance objectives as well, but in their case due to  
360 insufficient correlation between observations and simulations at the hourly scale. The site DUE is  
located in an industrial area, next to a busy highway, while FIL is located in a rural environment  
but next to a motorway intersection and the portals of the three tunnels of the motorway bypass in  
Zurich West. Incorrectly prescribed variability in related traffic and industrial emissions may explain  
the insufficient scores. Discrepancies between observations and simulations are further discussed in  
365 the following sections to identify error sources and propose possible model improvements.

Though fulfilling the quality objectives in most cases, the modelling system seems to generally  
overestimate concentrations at all observation locations. The overestimation might be attributed to  
incorrect emission magnitude in the inventories. However, when considering the minimum values  
within a 15 m horizontal and 2 m vertical distance, all performance scores at all sites are signifi-  
370 cantly improved. The biases almost vanish and the synthesis MQO index is smaller than 1 at almost  
all sites at the hourly and daily scale, and even below 0.5 on average. A MQO below 0.5 was consid-  
ered by Thunis et al. (2012) as a reference objective since observation errors start dominating model  
error below 0.5. The general improvement of the model performance when taking the minimum in  
a certain distance rather than values at the exact location of the observations suggests that the dis-  
375 persion of pollutants is generally underestimated, especially in the vicinity of emission hot spots.  
In fact, GRAL is known for overestimating pollutant concentrations near building façades (Oetli,  
2015b). In addition, traffic-induced turbulence is accounted for only by spreading traffic emissions  
over the lowest 3 m above ground (see Sect. 3.3). The better performance of the model in the mini-  
mum simulation at traffic sites suggests that additional efforts should be made to better parametrize  
380 the traffic-induced turbulence.

The temporal correlations between simulations and observations do not change drastically be-  
tween the two approaches, but also for this metric there is an improvement when using the minimum  
values in most cases. The correlations between observations and simulations are in the range 0.53–  
0.79 at the hourly scale and 0.71–0.94 at the daily scale. At most sites, these correlations are at  
385 least 0.5 higher than the correlations between observations and temporally varying emissions, which

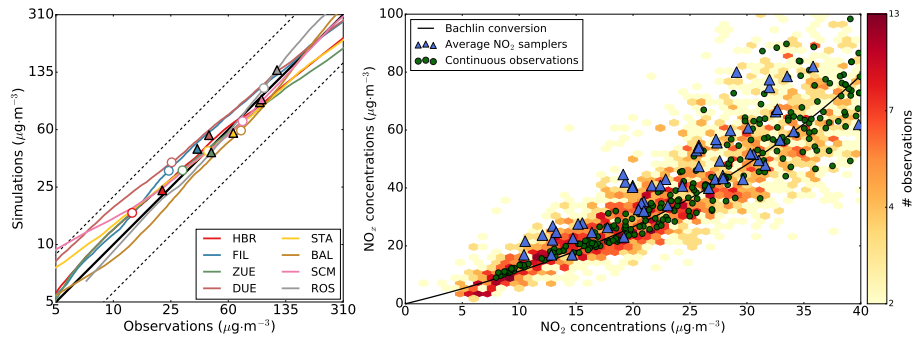


**Figure 3.** Comparison of observed and simulated  $\text{NO}_x$  and  $\text{NO}_2$  concentrations. (left) Quantile-quantile plot of hourly  $\text{NO}_x$  concentrations at continuous sites. The solid and dashed black lines are the 1:1 line and the 1:2 and 2:1 lines, respectively. Filled triangles are the 2013–2014 mean and empty circles the median concentrations. Note the logarithmic scale of the plot. (right) Concentrations at passive samplers. Yellow to red coloured background show the comparison between 2-weekly observed  $\text{NO}_2$  (x-axis) and corresponding simulated  $\text{NO}_x$  (y-axis). Triangles are the mean values per station averaged over the entire period 2013–2014. For comparison, green dots are the two-weekly averages of  $\text{NO}_2$  and  $\text{NO}_x$  as observed at continuous sites. The black line is a “Bachlin”-type parametrization of the ratio between  $\text{NO}_x$  to  $\text{NO}_2$  (Düring et al., 2011).

demonstrates that meteorological variability is a key factor driving the variability in concentrations and that this variability is very well captured by the catalogue-based modelling approach. Exceptions are the sites ROS, SCM and BAL for which the correlations are only 0.05 to 0.2 better than the emission-observation correlations. At these traffic sites the variability appears to be dominated  
 390 by traffic intensity rather than by meteorology.

In the following, we compare observations to the “minimum” simulations due to their significantly better performance, and will further discuss the implications of this choice in Sect. 5.

## 4.2 Evaluation of the spatial distribution

The average distribution of simulated  $\text{NO}_x$  concentrations is shown in Fig. 2. Apart from hills and  
 395 forest areas, where the concentrations are close to the background,  $\text{NO}_x$  concentrations are dominated by local emissions in most built-up areas. Large gradients exist between traffic corridors with concentrations higher than  $100 \mu\text{g}\cdot\text{m}^{-3}$  and backyards and smaller streets.

To evaluate the quality of this average distribution, we use eight continuous monitoring sites and 65  $\text{NO}_2$  passive samplers distributed rather uniformly over the city and covering the full range of  
 400 pollution levels. Figure 3 and Tab. 2 compare average observations with simulations. As shown by the quantile-quantile plot and the biases, there is no specific dependency of the mismatches on the concentrations. The fractional bias remains roughly the same (well below 50%) at all sites over the whole range of observed concentrations. As for the biases, it is considered that an air pollution model is performing well when the NMB is below 50% (e.g., Kumar et al., 2006). The relative bias only

405 seems to increase at all sites at the lower and upper end of the concentration range, suggesting higher uncertainties for very high and very low concentrations.

At passive sampler sites the comparison is complicated by the fact that the modelling system simulates  $\text{NO}_x$  whereas passive samplers measure  $\text{NO}_2$ . The ratio between  $\text{NO}_2$  and  $\text{NO}_x$  is often parametrized by a non-linear “Bachlin” function depending solely on the concentration of  $\text{NO}_x$  (e.g., Düring et al., 2011). The function accounts for the fact that the ratio tends to increase with increasing distance from the source and hence with decreasing  $\text{NO}_x$  concentration. The ratios between biweekly averaged  $\text{NO}_2$  and  $\text{NO}_x$  concentrations as measured at the continuous sites (green dots in Fig. 3) indeed closely follow a Bachlin curve, though with increasing spread at high  $\text{NO}_x$  concentrations. The ratios between the two-year averages of  $\text{NO}_2$  measured at the passive samplers and the corresponding simulated  $\text{NO}_x$  values follow this curve as well, although the simulated  $\text{NO}_x$  values tend to be somewhat too high. For the individual 2-weekly averages (coloured background in right panel of Fig. 3), this overestimation is particularly evident for the low concentrations. These low concentrations mainly occur during the summer season when the lifetime of  $\text{NO}_x$  is shortest. The overestimation of low concentrations could therefore be a result of treating  $\text{NO}_x$  as a passive tracer in the model not accounting for photochemical depletion. Furthermore, Steinbacher et al. (2007) demonstrated that  $\text{NO}_x$  concentrations at TAE, which are added as a background to our simulations, are generally overestimated by 3–4  $\mu\text{g}\cdot\text{m}^{-3}$  due to interferences of other reactive nitrogen compounds like PAN and  $\text{HNO}_3$  when using a molybdenum converter.

425 Apart from a possible overestimation of very low concentrations, our modelling system is able to reproduce the large spatial variations in average concentration levels with high confidence.

### 4.3 Evaluation of the temporal variability

Good scores for the average spatial distribution of air pollutant concentrations have already been demonstrated for other modelling systems (e.g., Soulhac et al., 2011; Di Sabatino et al., 2007). However, accurately reproducing not only average concentrations but also the temporal evolution from hourly to seasonal time scales is a much more challenging objective that has received little attention so far. This section therefore focusses on evaluating the simulated temporal variability.

#### 4.3.1 Example period

In Fig. 4, observations are compared to simulations for a selected period of time, October 2013. The period has been selected as the only time, when all sites were in operation, but also because the concentrations represented the average patterns of concentration variability rather than some specific pollution events. The simulations are divided into their main contributors (background, light and heavy duty traffic, heating systems and the rest). Sites are sorted following the average observed  $\text{NO}_x$  concentrations, from the highest at ROS to the lowest at HBR. Simulations at all sites are generally in very good agreement with observations: the diurnal cycle is mostly well reproduced and



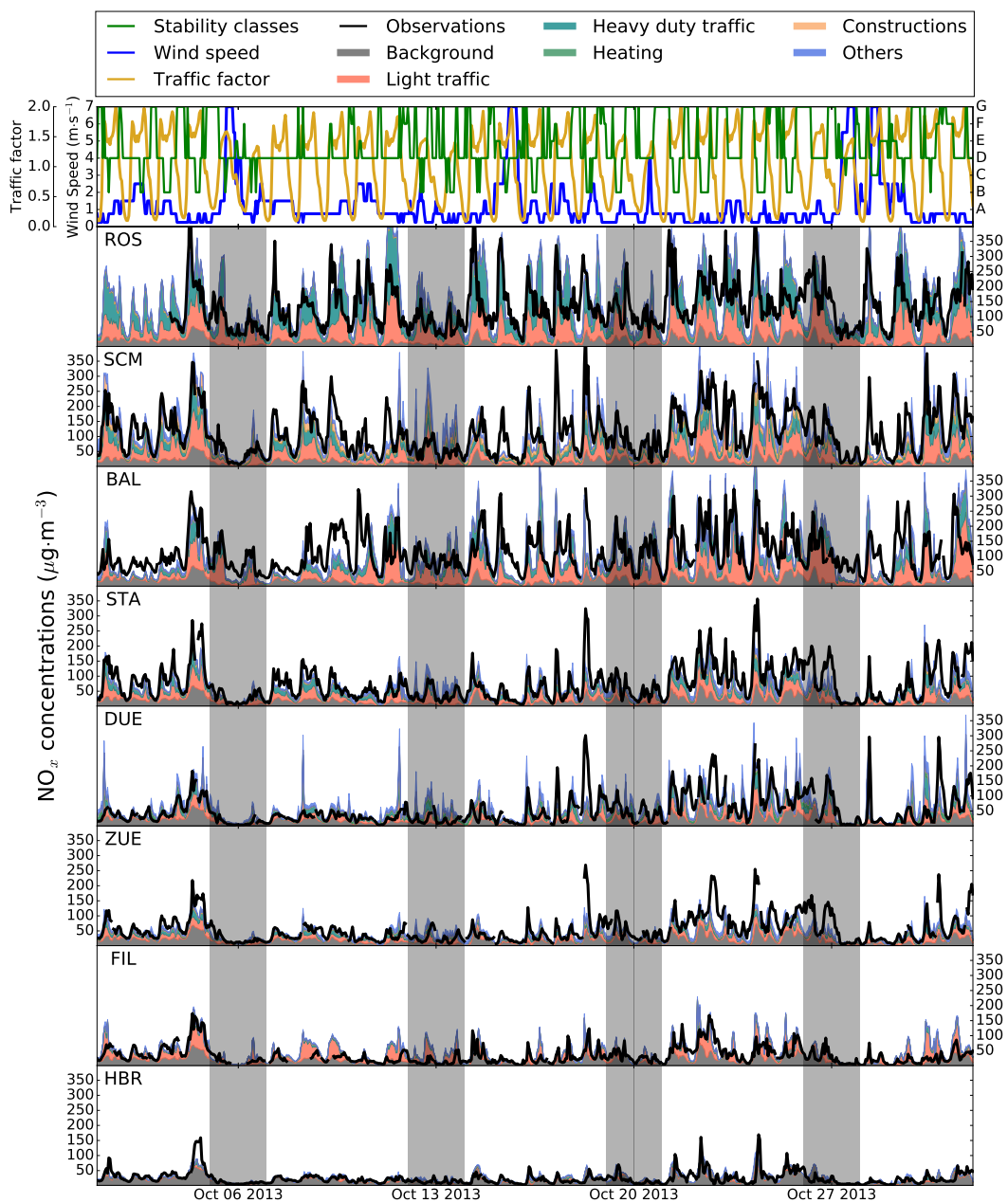


**Figure 4.** Hourly time series of observed and simulated concentrations at all sites for the month October 2013. Simulations are separated by contributions from the main emission categories (light traffic, heavy duty traffic, heating and the rest). Shaded periods represent week-ends. (top) Stability classes and wind categories of the hourly selected weather situations.

440 the different concentration patterns during weekends (shaded periods in Fig. 4) are well detected. Whereas background concentrations are the same at all sites and never exceed  $50 \mu\text{g}\cdot\text{m}^{-3}$ , the magnitude of local contributions varies significantly from one site to the other, very consistently with observations. FIL and HBR show almost no local contribution whereas street sites such as ROS and SCM are largely dominated by local traffic emissions. However, at the three most polluted sites, 445 ROS, SCM and STA, the simulations deviate significantly from the observations for some periods. As discussed earlier this is likely related to the large local gradients at these sites of  $30 \mu\text{g}\cdot\text{m}^{-3}$ ,  $59 \mu\text{g}\cdot\text{m}^{-3}$  and  $330 \mu\text{g}\cdot\text{m}^{-3}$  on average within a distance of 15 m at STA, SCM and ROS respectively.

At all sites, traffic emissions are the biggest contributor to air pollution. Since the variability of 450 traffic emissions does not change significantly from one day to the other (apart from the weekends), most of the concentration variability is attributable to changes in weather conditions, and this variability is generally well captured by the simulations. For instance, four events with strong winds (see wind speed in the upper panel of Fig. 4) and correspondingly low concentrations are well reproduced. Nevertheless, inconsistencies in the selection of weather situations occasionally appear 455 as suggested by sporadic peaks mostly at the site DUE, which appear in the simulations but not in the observations. Such events are most of the time not realistic and could point at a too frequent selection of very stable situations by the match-to-observation procedure. Such peaks may be amplified through the catalogue-based procedure, since particles emitted during a 1 h time span are fully attributed to the same hour in the steady-state assumptions, while some particles are transported 460 longer than 1 h. Still, a few short peaks are observed and reproduced, demonstrating the ability of the system to capture short-term changes in weather conditions.

At the site HBR, 200 m above the altitude of the city centre, the concentrations are dominated by the background and are in most cases well reproduced. However, in some very specific situations, the modelling system appears to miss some transport of pollution from the valley to higher altitudes. 465 For instance, a pollution event was observed at all sites on Oct. 4<sup>th</sup> in Fig. 4. It was well reproduced by the model at all sites with the exception of HBR, where the model only marginally deviated from the background, suggesting underestimated vertical transport from the city centre, or a mismatch in simulated wind directions at higher altitudes.

### 4.3.2 Complete two-year period

470 The entire period of simulation, covering the years 2013 and 2014, is presented in Fig. 5 similar to Fig. 4 but as daily instead of hourly averages. Synoptic variability characterized by periods of strong air pollutant accumulation alternating with cleaner periods is superimposed on a seasonal cycle with systematically higher concentrations during winter. The synoptic variability, which is manifested by varying contributions from emissions within the city with changing weather conditions, is very well 475 reproduced with good FAC2 scores and high correlation coefficients for daily averages ( $r = 0.86$  on

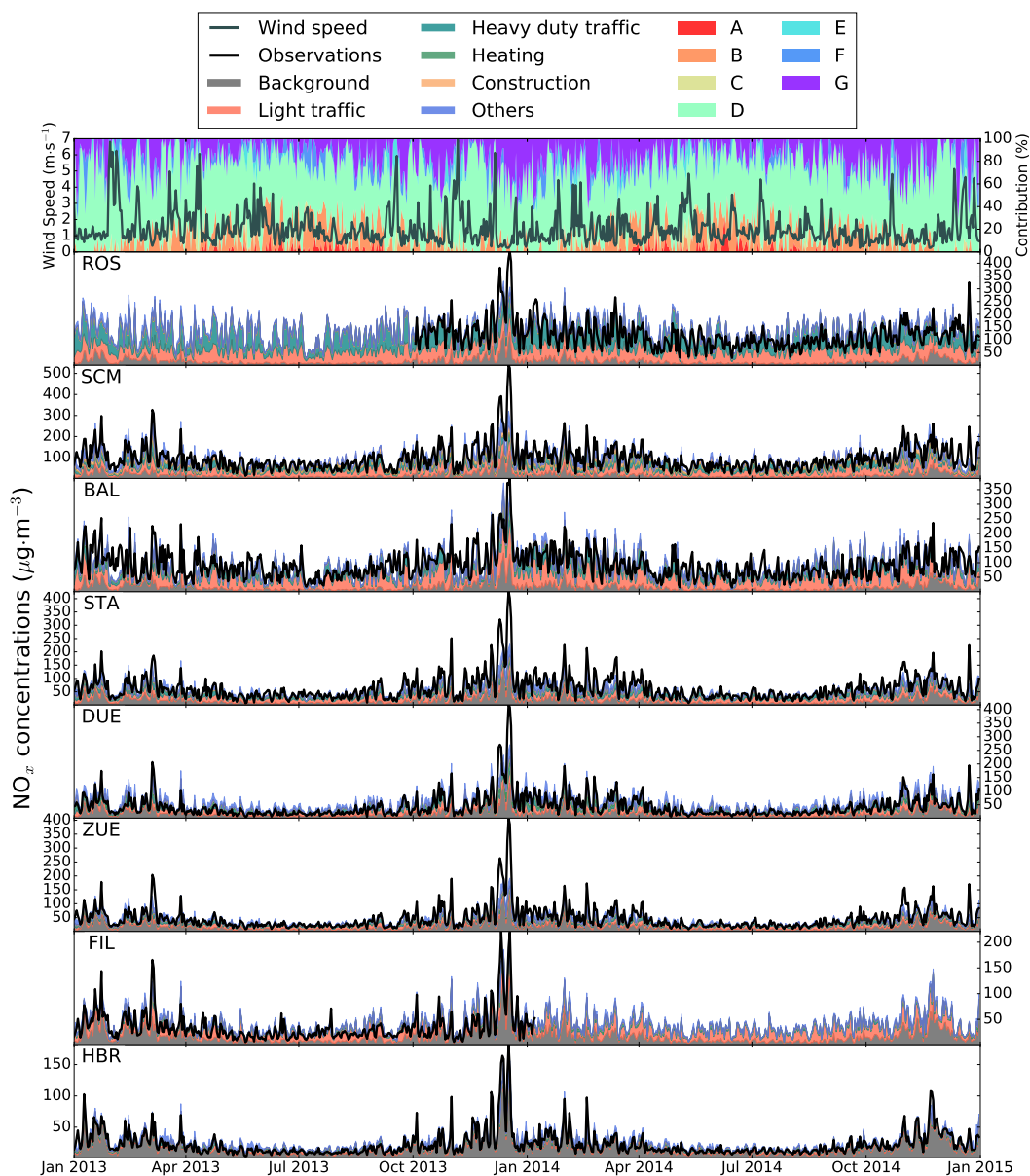


**Figure 5.** Daily observed and simulated concentrations at all observation sites for the years 2013 and 2014. Simulations are separated by contributions as in Fig. 4. (top) Daily averages of stability class contributions (A–G) and wind categories. Measurements at FIL were discontinued in January 2014, whereas the site ROS started being operated in October 2013.

average; see Tab. 2). At all sites, FAC2 and  $r$  scores are 10–20% higher at the daily scale than at the hourly scale, indicating that the synoptic variability is better captured than the diurnal cycle. Events of low concentrations are generally correlated with higher wind speeds whereas concentration peaks are associated with particularly stable situations (stability classes E to G).

480 Although heating systems dominantly emit during winter time, they contribute only marginally to the seasonal cycle of concentrations as simulated by the system. Indeed, all the observation sites are located close to the ground at 3–4 m, while heating emissions occur on building roofs and further rise after release, thus impacting ground concentrations only little. The seasonal cycle of  $\text{NO}_x$  concentrations is, thus, mostly driven by the vertical stability of the atmosphere rather than by the  
485 seasonal cycle of emissions. Convective situations are more frequent and pollutants are therefore mixed more effectively during summer, reducing ground concentrations, whereas they accumulate close to the surface in winter. Because of increased stable conditions,  $\text{NO}_x$  pollution events tend to be more severe in winter at all sites. Therefore, the background concentrations partly explain the seasonal cycle of city concentrations, especially in the background site HBR and during the strong  
490 pollution event in December 2013. Local contributions from traffic emissions dominate the seasonal variability at all other sites even though traffic emissions do not change significantly from one month to another.

In December 2013, a particularly strong pollution event occurred. During this month, observed daily averages reached up to  $700 \mu\text{g}\cdot\text{m}^{-3}$ , with values above  $200 \mu\text{g}\cdot\text{m}^{-3}$  at all sites. These very  
495 high concentrations are explained by the combination of regional recirculation of pollution (average background concentrations were  $48 \mu\text{g}\cdot\text{m}^{-3}$  for this month), low winds and highly stable conditions enhancing the urban contribution. The modelling system reasonably fills the gap between observed peaks and the background. However, it is unable to reach the observed peak concentrations at most sites. The accumulation of pollutants in the city likely occurred over a time scale of several  
500 hours, which our approach with steady-state hourly simulations is unable to reproduce. This approach underestimates air pollutant accumulation within the city during periods of particularly low wind speeds, since this local accumulation cannot be represented by the rural background and as particles crossing the domain borders cannot re-enter the limited-area domain. General improvements in the model set-up (e.g., higher spatial and temporal resolution and bigger domain) as well as in the  
505 method (temporal hysteresis from one hour to the next ones) will be needed to better reproduce such severe pollution events.

Figure 6 presents a general temporal evaluation (RMSEs and correlation coefficients) of the model at all passive samplers. Biweekly  $\text{NO}_2$  observations are compared to the corresponding  $\text{NO}_2$  values from the model obtained using the  $\text{NO}_x$  to  $\text{NO}_2$  conversion formula of Düring et al. (2011) (black  
510 line in Fig. 3). For reference, correlation coefficients and RMSEs have been calculated as well for different concentration intervals based on biweekly averages from continuous measurements of  $\text{NO}_2$  and  $\text{NO}_x$ , represented by the blue and green line in Fig. 6, respectively. These lines, which are only

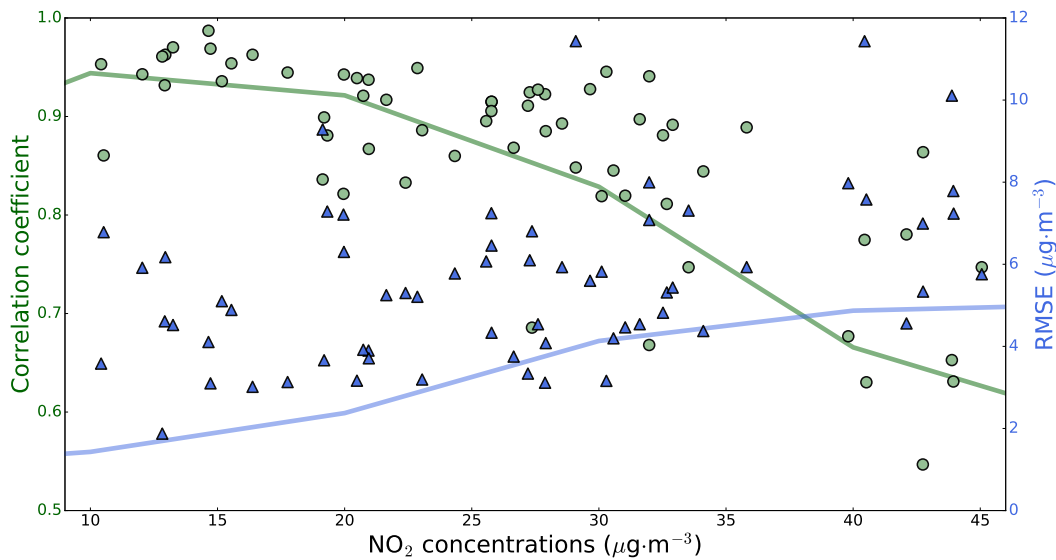


**Figure 6.** Correlation coefficients (green dots) and RMSE (blue triangles) at all passive samplers as a function of the mean  $\text{NO}_2$  concentration at each site for the two-year period 2013–2014.  $\text{NO}_x$  simulations are converted to  $\text{NO}_2$  using the parametrized conversion of Düring et al. (2011). The green and blue line corresponds to the correlation coefficient and RMSE respectively, as computed for  $5 \mu\text{g}\cdot\text{m}^{-3}$  wide sliding concentration intervals by comparing two-week averages of continuous  $\text{NO}_2$  observations with converted equivalents of observed  $\text{NO}_x$ .

based on observations, provide a measure of the uncertainties implied by the  $\text{NO}_x$ – $\text{NO}_2$  conversion alone and therefore of the best score achievable by the model. It appears that the two-weekly correlation coefficients are very similar to the uncertainties implied by the conversion, suggesting a very good agreement between observations and simulations, in agreement with the high correlations for the daily averages at the continuous sites in Tab. 2. The RMSEs are on average two times larger ( $3 \mu\text{g}\cdot\text{m}^{-3}$ ) than the conversion uncertainties. Contrary to RMSEs computed from continuous sites, RMSEs from converted simulations at passive sites do not show any clear dependency on concentration levels. This may partly be attributable to the systematic bias at the background site TAE for low concentrations (see Sect. 4.2).

### 4.3.3 Diurnal cycle of concentrations

Beyond the seasonal and daily variability, the diurnal cycle of concentrations plays a key role in assessing the exposure of the population to air pollution as people commute and spend their day at different locations within the city. The mean diurnal cycles of observations and simulations are presented in Fig. 7. Here, only weekdays are discussed as the diurnal cycle of emissions is more pronounced than during weekends. Consistent with the observations, the simulated concentrations are higher at daytime than during night, with a morning peak at all sites and a late afternoon peak at some sites.

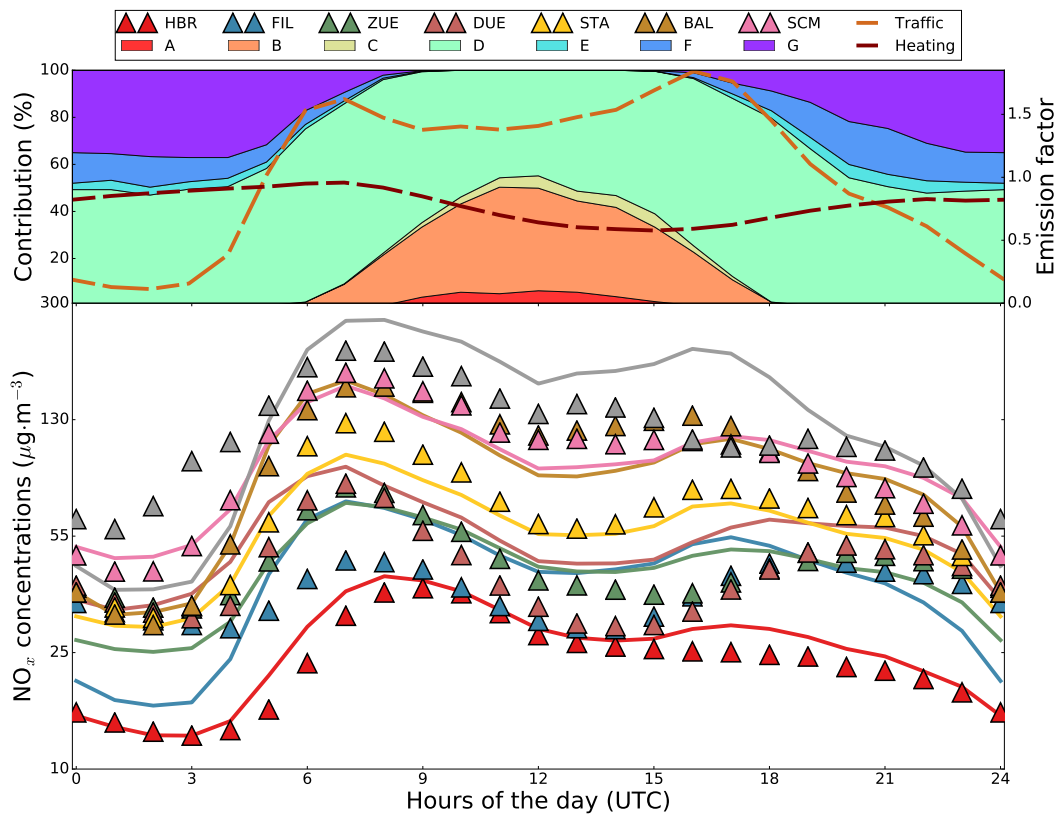


**Figure 7.** Two-year mean diurnal cycle of concentrations, traffic emissions and meteorology during weekdays. (top) Contributions of stability classes (A very unstable, D neutral, G very stable) to the hourly meteorology. The dashed lines are the emission profiles for light traffic and heating emissions. (bottom) Diurnal cycle of observed (triangles) and simulated  $\text{NO}_x$  concentrations (solid lines) at continuous measurement sites.

530 The morning rush hour leads to a stronger peak as the atmosphere is usually more stably stratified at this time of the day than during the evening rush hour. At most sites, both in the model and the observations, the peak occurs at 7 a.m. UTC, which corresponds to 8 a.m. local time in winter and 9 a.m. local time in summer. At HBR, the simulated and observed peaks happen later than at other sites. However, the observed peak is delayed by about one hour more than the simulated one.

535 As mentioned in Sect. 4.3.1, HBR is an elevated site with no significant emissions nearby. Thus, pollution emitted in the morning in the city appears to be transported to the site with a delay of 2–3 hours, while in the model, the steady-state assumption makes pollutants to be transported virtually faster.

After the morning peak, the observed concentrations follow three possible paths: a steady decrease  
 540 until the night time minimum (ROS, SCM, HBR), an afternoon plateau with a small peak around 4 p.m. (STA, BAL) at the same time as the afternoon traffic peak, or a plateau with a late evening concentration peak around 8–9 p.m. (FIL, DUE, ZUE). These patterns are correctly reproduced by

the model at the sites HBR, BAL, STA and DUE. At the other sites, the model simulates an afternoon plateau followed by a small peak from traffic contributions not consistent with observations.

545 The uniform scaling of traffic emissions is a strong simplification that likely contributes to the discrepancies between simulated and observed diurnal profiles at some sites: a closer analysis of the data from the 89 traffic counters, for example, showed that the traffic intensity remains constantly high at daytime in the city center whereas there are clear morning and evening peaks in the outer districts. In addition, some streets are more intensively used by incoming traffic (strong morning peak),  
550 others by outgoing traffic (strong evening peak). The late evening peak at 8–9 p.m. UTC. could be explained by late emissions such as a surge in domestic heating before the night not accounted for in our system. A second explanation for the absence of a late-evening peak in the simulations could be twofold: first,  $\text{NO}_x$  is transported in the model as a passive tracer whereas in reality it is depleted by reaction with OH radicals. OH concentrations are highest when  $\text{NO}_x$  is relatively low and solar radiation large (Ren et al., 2003), i.e., on sunny summer afternoons. The  $\text{NO}_x$  lifetime is then reduced  
555 to about 2–4 hours (e.g., Liu et al., 2016), and not accounting for this depletion will contribute to a positive model bias in the afternoon as seen especially at sites in the lower range of the concentration levels. Second, the observed late evening peak occurs well after the evening rush hour, suggesting that it is an integrated response due to accumulation of  $\text{NO}_x$  over several hours. Such effects are  
560 not represented by our steady-state approach where the concentrations are solely determined by the emissions of the actual hour.

During the night, observed concentrations at the sites BAL, DUE, ZUE, FIL and STA converge to a similar level, which is well reproduced by the model at BAL, DUE, and STA, but underestimated at ZUE and especially at FIL. A systematic underestimation at night is also observed at ROS, especially  
565 in the early morning hours. The sites ROS and FIL are located next to important traffic corridors which might be used during the night more heavily than other roads including heavy duty traffic. Heavy duty traffic is not allowed in Switzerland at night between 22.00 and 05.00 local time (20.00 – 03.00 UTC in summer) but uses the early morning before the main rush hour intensively. Therefore, heavy duty traffic emissions close to these sites might be underestimated in our system. A second  
570 explanation can also be the missing accumulation of pollutants at night similar to the late evening peak. Under stable nocturnal situations, pollutants are slowly dispersed and remain longer in the domain of simulation than during the day. Accounting for air pollution accumulation over more than one hour would help increase the nocturnal low concentrations.

## 5 Discussion and conclusions

575 A catalogue-based approach computed with the nested simulation system GRAMM/GRAL was applied to simulating hourly  $\text{NO}_x$  concentration maps at 10 m resolution for the years 2013–2014. The modelling system was evaluated with 8 continuous  $\text{NO}_x$  measurements sites and 65  $\text{NO}_2$  passive

sampler sites. The overall model performance was compliant with the objective criteria of the European air quality modelling framework FAIRMODE at both the hourly and the daily scale for most stations. The temporal variability of concentrations was well reproduced at the hourly, daily, two-weekly and seasonal scales. This can be explained to a minor extent by the proper representation of the variability in emissions, especially at the diurnal time scale, but it is mostly due to the successful representation of the meteorological variability by the catalogue-based approach. The diurnal cycle of concentrations, which is particularly critical to reproduce the pollution exposure of individuals commuting in the city, is largely consistent with the observations despite a systematic underestimation of concentrations during the night at some locations. The generally good performance of our system, on top of the reasonable computation costs and its flexibility (making it possible to carry out numerous simulation scenarios as it was done in Berchet et al., 2017), makes it a very suitable solution for designing informed air quality plans urgently needed at the city scale (Miranda et al., 2015).

Recent progress in parametrized approaches allows standard urban air pollution models to reach performances at the yearly or even monthly scale (e.g., ADMS-urban system; Dedele and Miskinyte, 2015) comparable to our approach. The model accuracy at diurnal to daily time scales, however, have hardly ever been analysed, which makes it very difficult to place our results in context but also demonstrates the uniqueness of the simulations presented in this work. At shorter temporal scales, our modelling system is still out-performed by very high resolution CFD models (Kumar et al., 2015a), but these systems are limited to small domains and short periods of time. Less complex systems such as SIRANE (Soulhac et al., 2012), solving the high-resolution flow only in street canyons and approximating the dispersion above the urban canopy as Gaussian plumes, perform similarly to our model, albeit at higher computational costs, limiting their application to periods of typically a few weeks only. Despite the usage of an extremely detailed emission inventory, our simulations are still significantly limited by the representation of emissions, since only standard temporal profiles were applied to most sources, which are unable to capture the large temporal dynamics of real emissions. Real-time emission models accounting for the influence of actual activities such as traffic density and energy consumption or environmental factors such as outdoor temperature affecting not only heating (whose intensity is already modulated by temperature in our model through heating-degree days) but also cold-start traffic emissions (as suggested by the Handbook of Emission Factors for Road Transport v3.3; Keller et al., 2017) could further advance the representation of emissions variability in the future. Such emission models and complementary influence on emission variability could be informed for instance by mobile phone data and sensor networks. Such improved inputs proved to significantly increase the performance in other models (e.g., Soulhac et al., 2012; Borrego et al., 2016). The main gain of the catalogue-based method is, above all, the reduced computational cost allowing for high-resolution simulations of long time periods with a time resolution down to



one hour. Further developments are required to improve this approach by replacing fixed emission  
615 patterns by transient ones, obtained for instance with suitable traffic models.

A general overestimation of concentrations was found at all sites in our model, mostly related to  
insufficient dispersion in the model as well as to unrealistic accumulation of pollutants near buildings  
façades, which have a strong impact on simulations with the chosen 10 m horizontal resolution. The  
apparently too low dispersion may be related to the fact that traffic-induced turbulence is only crudely  
620 represented. Some limitations of the catalogue-based method were revealed, which are attributable  
to the steady-state assumption and the limited model domain. Particles that have been transported  
in the city for more than an hour are assigned to the same hour they were released in the current  
version of the system. Future versions should account for the particle transport age, which can be  
made accessible in the GRAL model outputs. This would likely smooth out some of the unrealistic  
625 short peaks produced in our simulations. A long residence time of particles in the simulation domain  
can also have implications in terms of chemistry.  $\text{NO}_x$  depletion due to oxidation by OH radicals  
or night time  $\text{N}_2\text{O}_5$  chemistry was neglected in our system, as the typical lifetime of  $\text{NO}_x$  in the  
atmosphere is never shorter than a few hours (during sunny summer afternoon; Liu et al., 2016).  
Accounting for long residence times in the simulation domain may allow us to compute simplified  
630 chemical reactions within the frame of the catalogue-based approach.

As demonstrated in this study, our model system produces a very realistic representation of the  
spatial distribution and temporal variability of  $\text{NO}_x$  in the city, which makes it a highly suitable  
tool for policy makers. The city of Zurich is indeed implementing the system as a new tool for  
improved air pollution control and urban planning. So far, our simulations have been generated  
635 without any input from actual air pollution measurements. Incorporating such observations through  
data assimilation and machine learning methods could further enhance the quality of the model  
predictions and even better satisfy the requirements of epidemiological studies, which need to be  
based on accurate, unbiased data. The selection of weather situations in the catalogue could also  
benefit from assimilating concentration observations in the system, instead of wind and radiation  
640 observations only. Additional meteorological observations not directly related to the definition of  
the catalogue, such as turbulence fluxes, temperature gradients or boundary layer height, are also  
increasingly available and might improve the selection of weather situations in the catalogue as well.  
A fully integrated high-resolution modelling system would enable short- and long-term pollutant and  
greenhouse gas monitoring in cities for subsequent use in the development of mitigation strategies.

645 Finally,  $\text{NO}_x$  concentrations are relevant for regulation purposes only as a proxy of  $\text{NO}_2$  concen-  
trations. Oettl and Uhrner (2011) introduced a chemical module to GRAL, but the transient-based  
approach of this module with explicit computation of  $\text{O}_3$  3-dimensional fields prevents benefiting  
from the reduced computation costs of the catalogue-based approach. An intermediate system, ac-  
counting for the average distribution of particle age and rough estimates of  $\text{O}_3$  concentrations, should  
650 be tested in future to reproduce  $\text{NO}_2$  concentrations at fine scales in cities.

## Code and data availability

The system GRAMM/GRAL is made available by the Technische Universität Graz on the following webpage: [lampx.tugraz.at/gral/index.php](http://lampx.tugraz.at/gral/index.php). The catalogue-based method is fully described in Berchet et al. (2017) and related Python scripts can be requested to the corresponding author.

655 *Acknowledgements.* We thank the City of Zurich for the building and emission inventory in Zurich, as well as  
their pollution monitoring network. We thank the cantonal environment office for sharing emission information  
and pollution observations We thank MeteoSwiss and the Swiss Ministry for the Environment for providing data  
from their permanent measurement networks. We thank the reviewers for their fruitful comments to improve  
our manuscript. This work was financed by the Swiss National Fund in the framework of the NanoTera project  
660 OpenSense2 and by the City of Zurich.

## References

- Almbauer, R. A., Oetl, D., Bacher, M., and Sturm, P. J.: Simulation of the air quality during a field study for the city of Graz, *Atmospheric Environment*, 34, 4581–4594, doi:10.1016/S1352-2310(00)00264-8, <http://www.sciencedirect.com/science/article/pii/S1352231000002648>, 2000.
- 665 Anfossi, D., Alessandrini, S., Trini Castelli, S., Ferrero, E., Oetl, D., and Degrazia, G.: Tracer dispersion simulation in low wind speed conditions with a new 2D Langevin equation system, *Atmospheric Environment*, 40, 7234–7245, doi:10.1016/j.atmosenv.2006.05.081, <http://www.sciencedirect.com/science/article/pii/S135223100600673X>, 2006.
- 670 Beelen, R., Hoek, G., van den Brandt, P. A., Goldbohm, R. A., Fischer, P., Schouten, L. J., Jerrett, M., Hughes, E., Armstrong, B., and Brunekreef, B.: Long-Term Effects of Traffic-Related Air Pollution on Mortality in a Dutch Cohort (NLCS-AIR Study), *Environ Health Perspect*, 116, 196–202, doi:10.1289/ehp.10767, <http://www.ncbi.nlm.nih.gov/pmc/articles/PMC2235230/>, 2008.
- 675 Beelen, R., Voogt, M., Duyzer, J., Zandveld, P., and Hoek, G.: Comparison of the performances of land use regression modelling and dispersion modelling in estimating small-scale variations in long-term air pollution concentrations in a Dutch urban area, *Atmospheric Environment*, 44, 4614–4621, doi:10.1016/j.atmosenv.2010.08.005, <http://www.sciencedirect.com/science/article/pii/S1352231010006588>, 2010.
- 680 Beelen, R., Hoek, G., Vienneau, D., Eeftens, M., Dimakopoulou, K., Pedeli, X., Tsai, M.-Y., Künzli, N., Schikowski, T., Marcon, A., Eriksen, K. T., Raaschou-Nielsen, O., Stephanou, E., Patelarou, E., Lanki, T., Yli-Tuomi, T., Declercq, C., Falq, G., Stempfelet, M., Birk, M., Cyrus, J., von Klot, S., N'ador, G., Varr'ò, M. J., Dedele, A., Grazuleviciene, R., Mölter, A., Lindley, S., Madsen, C., Cesaroni, G., Ranzi, A., Badaloni, C., Hoffmann, B., Nonnemacher, M., Krämer, U., Kuhlbusch, T., Cirach, M., de Nazelle, A., Nieuwenhuijsen, M., Bellander, T., Korek, M., Olsson, D., Strömgren, M., Dons, E., Jerrett, M., Fischer, P., Wang, M., Brunekreef, B., and de Hoogh, K.: Development of NO<sub>2</sub> and NO<sub>x</sub> land use regression models  
685 for estimating air pollution exposure in 36 study areas in Europe – The ESCAPE project, *Atmospheric Environment*, 72, 10–23, doi:10.1016/j.atmosenv.2013.02.037, <http://www.sciencedirect.com/science/article/pii/S1352231013001386>, 2013.
- 690 Beelen, R., Raaschou-Nielsen, O., Stafoggia, M., Andersen, Z. J., Weinmayr, G., Hoffmann, B., Wolf, K., Samoli, E., Fischer, P., Nieuwenhuijsen, M., Vineis, P., Xun, W. W., Katsouyanni, K., Dimakopoulou, K., Oudin, A., Forsberg, B., Modig, L., Havulinna, A. S., Lanki, T., Turunen, A., Oftedal, B., Nystad, W., Nafstad, P., De Faire, U., Pedersen, N. L., Östenson, C.-G., Fratiglioni, L., Penell, J., Korek, M., Pershagen, G., Eriksen, K. T., Overvad, K., Ellermann, T., Eeftens, M., Peeters, P. H., Meliefste, K., Wang, M., Bueno-de Mesquita, B., Sugiri, D., Krämer, U., Heinrich, J., de Hoogh, K., Key, T., Peters, A., Hampel, R., Concin, H., Nagel, G., Ineichen, A., Schaffner, E., Probst-Hensch, N., Künzli, N., Schindler, C., Schikowski, T.,  
695 Adam, M., Phuleria, H., Vilier, A., Clavel-Chapelon, F., Declercq, C., Gironi, S., Krogh, V., Tsai, M.-Y., Ricceri, F., Sacerdote, C., Galassi, C., Migliore, E., Ranzi, A., Cesaroni, G., Badaloni, C., Forastiere, F., Tamayo, I., Amiano, P., Dorronsoro, M., Katsoulis, M., Trichopoulou, A., Brunekreef, B., and Hoek, G.: Effects of long-term exposure to air pollution on natural-cause mortality: an analysis of 22 European cohorts within the multicentre ESCAPE project, *The Lancet*, 383, 785–795, doi:10.1016/S0140-6736(13)62158-3,  
700 [http://www.thelancet.com/journals/lancet/article/PIIS0140-6736\(13\)62158-3/abstract](http://www.thelancet.com/journals/lancet/article/PIIS0140-6736(13)62158-3/abstract), 2014.

- Berchet, A., Zink, K., Muller, C., Oetl, D., Brunner, J., Emmenegger, L., and Brunner, D.: A cost-effective method for simulating city-wide air flow and pollutant dispersion at building resolving scale, *Atmospheric Environment*, doi:10.1016/j.atmosenv.2017.03.030, <http://www.sciencedirect.com/science/article/pii/S1352231017301620>, 2017.
- 705 Borrego, C., Amorim, J. H., Tchepel, O., Dias, D., Rafael, S., Sá, E., Pimentel, C., Fontes, T., Fernandes, P., Pereira, S. R., Bandeira, J. M., and Coelho, M. C.: Urban scale air quality modelling using detailed traffic emissions estimates, *Atmospheric Environment*, 131, 341–351, doi:10.1016/j.atmosenv.2016.02.017, <http://www.sciencedirect.com/science/article/pii/S1352231016301285>, 2016.
- 710 Brandt, J., Silver, J. D., Christensen, J. H., Andersen, M. S., Bønløkke, J. H., Sigsgaard, T., Geels, C., Gross, A., Hansen, A. B., Hansen, K. M., Hedegaard, G. B., Kaas, E., and Frohn, L. M.: Contribution from the ten major emission sectors in Europe and Denmark to the health-cost externalities of air pollution using the EVA model system – an integrated modelling approach, *Atmos. Chem. Phys.*, 13, 7725–7746, doi:10.5194/acp-13-7725-2013, <http://www.atmos-chem-phys.net/13/7725/2013/>, 2013.
- 715 Briant, R., Seigneur, C., Gadrat, M., and Bugajny, C.: Evaluation of roadway Gaussian plume models with large-scale measurement campaigns, *Geosci. Model Dev.*, 6, 445–456, doi:10.5194/gmd-6-445-2013, <http://www.geosci-model-dev.net/6/445/2013/>, 2013.
- Brunekreef, B. and Holgate, S. T.: Air pollution and health, *The Lancet*, 360, 1233–1242, doi:10.1016/S0140-6736(02)11274-8, <http://www.sciencedirect.com/science/article/pii/S0140673602112748>, 2002.
- 720 Cohen, A. J., Anderson, H. R., Ostro, B., Pandey, K. D., Krzyzanowski, M., Künzli, N., Gutschmidt, K., Pope III, C. A., Romieu, I., Samet, J. M., and others: Urban air pollution, *Comparative quantification of health risks*, 2, 1353–1433, <http://cdrwww.who.int/publications/cra/chapters/volume2/1353-1434.pdf>, 2004.
- Dedele, A. and Miskinyte, A.: The statistical evaluation and comparison of ADMS-Urban model for the prediction of nitrogen dioxide with air quality monitoring network, *Environ Monit Assess*, 187, 578, doi:10.1007/s10661-015-4810-1, <https://link.springer.com/article/10.1007/s10661-015-4810-1>, 2015.
- 725 Di Sabatino, S., Buccolieri, R., Pulvirenti, B., and Britter, R.: Simulations of pollutant dispersion within idealised urban-type geometries with CFD and integral models, *Atmospheric Environment*, 41, 8316–8329, doi:10.1016/j.atmosenv.2007.06.052, <http://www.sciencedirect.com/science/article/pii/S1352231007005791>, 2007.
- 730 Di Sabatino, S., Buccolieri, R., and Salizzoni, P.: Recent advancements in numerical modelling of flow and dispersion in urban areas: a short review, *International Journal of Environment and Pollution*, 52, 172–191, doi:10.1504/IJEP.2013.058454, <http://www.inderscienceonline.com/doi/abs/10.1504/IJEP.2013.058454>, 2013.
- 735 Düring, I., Bächlin, W., Ketzler, M., Baum, A., Friedrich, U., and Würzler, S.: A new simplified NO/NO<sub>2</sub> conversion model under consideration of direct NO<sub>2</sub>-emissions, *Meteorologische Zeitschrift*, 20, 67–73, doi:10.1127/0941-2948/2011/0491, <http://openurl.ingenta.com/content/xref?genre=article&issn=0941-2948&volume=20&issue=1&spage=67>, 2011.
- Duvall, R. M., Long, R. W., Beaver, M. R., Kronmiller, K. G., Wheeler, M. L., and Szykman, J. J.: Performance Evaluation and Community Application of Low-Cost Sensors for Ozone and Nitrogen Dioxide, *Sensors*, 16, 1698, doi:10.3390/s16101698, <http://www.mdpi.com/1424-8220/16/10/1698>, 2016.

- 740 EC: Directive 2008/50/EC of the European Parliament and of the Council of 21 May 2008 on ambient air quality and cleaner air for Europe, Tech. rep., Official Journal L 152, [http://ec.europa.eu/environment/air/quality/legislation/existing\\_leg.htm](http://ec.europa.eu/environment/air/quality/legislation/existing_leg.htm), 2001.
- FOEN: Pollutant Emissions from Road Transport, 1990 to 2035, Tech. rep., Federal Office for the Environment, Bern, <http://www.bafu.admin.ch/publikationen/publikation/01565/index.html?lang=en>, 2010.
- 745 Gao, Y., Dong, W., Guo, K., Liu, X., Chen, Y., Liu, X., Bu, J., and Chen, C.: Mosaic: A low-cost mobile sensing system for urban air quality monitoring, in: IEEE INFOCOM 2016 - The 35th Annual IEEE International Conference on Computer Communications, pp. 1–9, doi:10.1109/INFOCOM.2016.7524478, 2016.
- Hasenfratz, D., Saukh, O., Walser, C., Hueglin, C., Fierz, M., Arn, T., Beutel, J., and Thiele, L.: Deriving high-resolution urban air pollution maps using mobile sensor nodes, *Pervasive and Mobile Computing*, 16, Part B, 268–285, doi:10.1016/j.pmcj.2014.11.008, <http://www.sciencedirect.com/science/article/pii/S1574119214001928>, 2015.
- 750 Heimann, I., Bright, V. B., McLeod, M. W., Mead, M. I., Popoola, O. A. M., Stewart, G. B., and Jones, R. L.: Source attribution of air pollution by spatial scale separation using high spatial density networks of low cost air quality sensors, *Atmospheric Environment*, 113, 10–19, doi:10.1016/j.atmosenv.2015.04.057, <http://www.sciencedirect.com/science/article/pii/S1352231015300583>, 2015.
- 755 Heldstab, J., Leippert, F., Wuethrich, P., and Kuenzle, T.: NO<sub>2</sub> ambient concentrations in Switzerland. Modelling results for 2005, 2010, 2015, Tech. Rep. 1123, Federal Office for the Environment, Bern, Switzerland, <http://www.bafu.admin.ch/publikationen/publikation/01634/index.html?lang=en>, 2011.
- Heldstab, J., Schaeppli, B., Weber, F., and Sommerhalder, M.: Switzerland’s Informative Inventory Report, Tech. rep., Federal Office for the Environment, Bern, [http://www.bafu.admin.ch/luft/11017/11024/11592/index.html?lang=de&download=NHZLpZeg7t,lnp6I0NTU042l2Z6ln1acy4Zn4Z2qZpnO2Yuq2Z6gpJCGeoN\\_e2ym162epYbg2c\\_JjKbNoKSn6A--](http://www.bafu.admin.ch/luft/11017/11024/11592/index.html?lang=de&download=NHZLpZeg7t,lnp6I0NTU042l2Z6ln1acy4Zn4Z2qZpnO2Yuq2Z6gpJCGeoN_e2ym162epYbg2c_JjKbNoKSn6A--), 2016.
- Hurley, P. J., Physick, W. L., and Luhar, A. K.: TAPM: a practical approach to prognostic meteorological and air pollution modelling, *Environmental Modelling & Software*, 20, 737–752, doi:10.1016/j.envsoft.2004.04.006, <http://www.sciencedirect.com/science/article/pii/S1364815204001100>, 2005.
- 765 Jerrett, M., Arain, A., Kanaroglou, P., Beckerman, B., Potoglou, D., Sahuvaroglu, T., Morrison, J., and Giovis, C.: A review and evaluation of intraurban air pollution exposure models, *J Expo Anal Environ Epidemiol*, 15, 185–204, doi:10.1038/sj.jea.7500388, <http://www.nature.com/jes/journal/v15/n2/abs/7500388a.html>, 2004.
- 770 Jiao, W., Hagler, G., Williams, R., Sharpe, R., Brown, R., Garver, D., Judge, R., Caudill, M., Rickard, J., Davis, M., Weinstock, L., Zimmer-Dauphinee, S., and Buckley, K.: Community Air Sensor Network (CAIRSENSE) project: evaluation of low-cost sensor performance in a suburban environment in the southeastern United States, *Atmos. Meas. Tech.*, 9, 5281–5292, doi:10.5194/amt-9-5281-2016, <http://www.atmos-meas-tech.net/9/5281/2016/>, 2016.
- 775 Kakosimos, K. E., Hertel, O., Ketzler, M., and Berkowicz, R.: Operational Street Pollution Model (OSPM) – a review of performed application and validation studies, and future prospects, *Environ. Chem.*, 7, 485–503, doi:10.1071/EN10070, <http://www.publish.csiro.au/en/EN10070>, 2010.

- Keller, M., Hausberger, S., Matzer, C., Wüthrich, P., and Notter, B.: Handbuch für Emissionsfaktoren des Strassenverkehrs (HBEFA) (handbook of emission factors for road traffic). Version 3.3., Tech. rep., INFRAS AG, Bern, Switzerland, [http://www.hbefa.net/e/documents/HBEFA33\\_Documentation\\_20170425.pdf](http://www.hbefa.net/e/documents/HBEFA33_Documentation_20170425.pdf), 2017.
- 780 Kuenen, J., Denier van der Gon, H., Visschedijk, A., Van der Brugh, H., and Van Gijlswijk, R.: MACC European emission inventory for the years 2003–2007, TNO-report TNO-060-UT-2011-00588, Utrecht, [https://gmes-atmosphere.eu/documents/deliverables/d-emis/TNO\\_report\\_UT-00588\\_MACC\\_emission2003\\_2007.pdf](https://gmes-atmosphere.eu/documents/deliverables/d-emis/TNO_report_UT-00588_MACC_emission2003_2007.pdf), 2011.
- 785 Kumar, A., Dixit, S., Varadarajan, C., Vijayan, A., and Masuraha, A.: Evaluation of the AERMOD dispersion model as a function of atmospheric stability for an urban area, *Environ. Prog.*, 25, 141–151, doi:10.1002/ep.10129, <http://onlinelibrary.wiley.com/doi/10.1002/ep.10129/abstract>, 2006.
- Kumar, P., Garmory, A., Ketznel, M., Berkowicz, R., and Britter, R.: Comparative study of measured and modelled number of nanoparticles in an urban street canyon, *Atmospheric Environment*, 43, 949–958, doi:10.1016/j.atmosenv.2008.10.025, [//www.sciencedirect.com/science/article/pii/S1352231008009825](http://www.sciencedirect.com/science/article/pii/S1352231008009825), 2009.
- 790 Kumar, P., Ketznel, M., Vardoulakis, S., Pirjola, L., and Britter, R.: Dynamics and dispersion modelling of nanoparticles from road traffic in the urban atmospheric environment—A review, *Journal of Aerosol Science*, 42, 580–603, doi:10.1016/j.jaerosci.2011.06.001, <http://www.sciencedirect.com/science/article/pii/S0021850211000887>, 2011.
- 795 Kumar, P., Feiz, A.-A., Ngae, P., Singh, S. K., and Issartel, J.-P.: CFD simulation of short-range plume dispersion from a point release in an urban like environment, *Atmospheric Environment*, 122, 645–656, doi:10.1016/j.atmosenv.2015.10.027, <http://www.sciencedirect.com/science/article/pii/S1352231015304465>, 2015a.
- 800 Kumar, P., Morawska, L., Martani, C., Biskos, G., Neophytou, M., Di Sabatino, S., Bell, M., Norford, L., and Britter, R.: The rise of low-cost sensing for managing air pollution in cities, *Environment International*, 75, 199–205, doi:10.1016/j.envint.2014.11.019, <http://www.sciencedirect.com/science/article/pii/S0160412014003547>, 2015b.
- Lefebvre, W., Vercauteren, J., Schrooten, L., Janssen, S., Degraeuwe, B., Maenhaut, W., de Vlieger, I., Vankerkom, J., Cosemans, G., Mensink, C., Veldeman, N., Deutsch, F., Van Looy, S., Peelaerts, W., and Lefebvre, F.: Validation of the MIMOSA-AURORA-IFDM model chain for policy support: Modeling concentrations of elemental carbon in Flanders, *Atmospheric Environment*, 45, 6705–6713, doi:10.1016/j.atmosenv.2011.08.033, <http://www.sciencedirect.com/science/article/pii/S1352231011008570>, 2011.
- 805 Lelieveld, J., Barlas, C., Giannadaki, D., and Pozzer, A.: Model calculated global, regional and megacity premature mortality due to air pollution, *Atmos. Chem. Phys.*, 13, 7023–7037, doi:10.5194/acp-13-7023-2013, <http://www.atmos-chem-phys.net/13/7023/2013/>, 2013.
- 810 Li, X.-X., Liu, C.-H., Leung, D. Y. C., and Lam, K. M.: Recent progress in CFD modelling of wind field and pollutant transport in street canyons, *Atmospheric Environment*, 40, 5640–5658, doi:10.1016/j.atmosenv.2006.04.055, <http://www.sciencedirect.com/science/article/pii/S1352231006004559>, 2006.
- 815

- Liu, F., Beirle, S., Zhang, Q., Dörner, S., He, K., and Wagner, T.: NO<sub>x</sub> lifetimes and emissions of cities and power plants in polluted background estimated by satellite observations, *Atmos. Chem. Phys.*, 16, 5283–5298, doi:10.5194/acp-16-5283-2016, <http://www.atmos-chem-phys.net/16/5283/2016/>, 2016.
- 820 Miranda, A., Silveira, C., Ferreira, J., Monteiro, A., Lopes, D., Relvas, H., Borrego, C., and Roebeling, P.: Current air quality plans in Europe designed to support air quality management policies, *Atmospheric Pollution Research*, 6, 434–443, doi:10.5094/APR.2015.048, <http://www.sciencedirect.com/science/article/pii/S1309104215302129>, 2015.
- Mueller, M. D., Wagner, M., Barmpadimos, I., and Hueglin, C.: Two-week NO<sub>2</sub> maps for the City of Zurich, Switzerland, derived by statistical modelling utilizing data from a routine passive diffusion sampler network, *Atmospheric Environment*, 106, 1–10, doi:10.1016/j.atmosenv.2015.01.049, <http://www.sciencedirect.com/science/article/pii/S1352231015000722>, 2015.
- 825 Mueller, M. D., Hasenfratz, D., Saukh, O., Fierz, M., and Hueglin, C.: Statistical modelling of particle number concentration in Zurich at high spatio-temporal resolution utilizing data from a mobile sensor network, *Atmospheric Environment*, 126, 171–181, doi:10.1016/j.atmosenv.2015.11.033, <http://www.sciencedirect.com/science/article/pii/S1352231015305409>, 2016.
- 830 Oettl, D.: High resolution maps of nitrogen dioxide for the Province of Styria, Austria, *International Journal of Environment and Pollution*, 54, 137, doi:10.1504/IJEP.2014.065114, <http://www.inderscience.com/link.php?id=65114>, 2014.
- 835 Oettl, D.: A multiscale modelling methodology applicable for regulatory purposes taking into account effects of complex terrain and buildings on pollutant dispersion: a case study for an inner Alpine basin, *Environ Sci Pollut Res*, 22, 17 860–17 875, doi:10.1007/s11356-015-4966-9, <http://link.springer.com/article/10.1007/s11356-015-4966-9>, 2015a.
- Oettl, D.: Quality assurance of the prognostic, microscale wind-field model GRAL 14.8 using wind-tunnel data provided by the German VDI guideline 3783-9, *Journal of Wind Engineering and Industrial Aerodynamics*, 142, 104–110, doi:10.1016/j.jweia.2015.03.014, <http://www.sciencedirect.com/science/article/pii/S0167610515000744>, 2015b.
- 840 Oettl, D.: Documentation of the GRAMM mesoscale model Vs. 16.1, Tech. rep., Amt der Steiermaerkischen Landesregierung, Rep. LU-05-16, Graz, Austria, [http://app.luis.steiermark.at/berichte/Download/Fachberichte/Lu\\_05\\_16\\_GRAMM\\_Documentation.pdf](http://app.luis.steiermark.at/berichte/Download/Fachberichte/Lu_05_16_GRAMM_Documentation.pdf), 2016.
- 845 Oettl, D. and Hausberger, S.: Simulation of traffic induced No<sub>x</sub> -concentrations near the A 12 highway in Austria, *Atmospheric Environment - ATMOS ENVIRON*, 40, 6043–6052, doi:10.1016/j.atmosenv.2005.12.034, 2006.
- Oettl, D. and Uhrner, U.: Development and evaluation of GRAL-C dispersion model, a hybrid Eulerian–Lagrangian approach capturing NO–NO<sub>2</sub>–O<sub>3</sub> chemistry, *Atmospheric Environment*, 45, 839–847, doi:10.1016/j.atmosenv.2010.11.028, <http://www.sciencedirect.com/science/article/pii/S1352231010009957>, 2011.
- 850 Oettl, D., Sturm, P. J., Bacher, M., Pretterhofer, G., and Almbauer, R. A.: A simple model for the dispersion of pollutants from a road tunnel portal, *Atmospheric Environment*, 36, 2943–2953, doi:10.1016/S1352-2310(02)00254-6, <http://www.sciencedirect.com/science/article/pii/S1352231002002546>, 2002.
- 855

- Ottosen, T.-B., Kakosimos, K. E., Johansson, C., Hertel, O., Brandt, J., Skov, H., Berkowicz, R., Ellermann, T., Jensen, S. S., and Ketzel, M.: Analysis of the impact of inhomogeneous emissions in the Operational Street Pollution Model (OSPM), *Geosci. Model Dev.*, 8, 3231–3245, doi:10.5194/gmd-8-3231-2015, <http://www.geosci-model-dev.net/8/3231/2015/>, 2015.
- 860 Parra, M. A., Santiago, J. L., Martín, F., Martilli, A., and Santamaría, J. M.: A methodology to urban air quality assessment during large time periods of winter using computational fluid dynamic models, *Atmospheric Environment*, 44, 2089–2097, doi:10.1016/j.atmosenv.2010.03.009, <http://www.sciencedirect.com/science/article/pii/S1352231010002049>, 2010.
- Pernigotti, D., Gerboles, M., Belis, C. A., and Thunis, P.: Model quality objectives based  
865 on measurement uncertainty. Part II: NO<sub>2</sub> and PM<sub>10</sub>, *Atmospheric Environment*, 79, 869–878, doi:10.1016/j.atmosenv.2013.07.045, <http://www.sciencedirect.com/science/article/pii/S1352231013005761>, 2013.
- Raaschou-Nielsen, O., Andersen, Z. J., Beelen, R., Samoli, E., Stafoggia, M., Weinmayr, G., Hoffmann, B., Fischer, P., Nieuwenhuijsen, M. J., Brunekreef, B., Xun, W. W., Katsouyanni, K., Dimakopoulou, K., Sommar, J., Forsberg, B., Modig, L., Oudin, A., Oftedal, B., Schwarze, P. E., Nafstad, P., De Faire, U., Pedersen, N. L., Östenson, C.-G., Fratiglioni, L., Penell, J., Korek, M., Pershagen, G., Eriksen, K. T., Sørensen, M., Tjønneland, A., Ellermann, T., Eeftens, M., Peeters, P. H., Meliefste, K., Wang, M., Bueno-de Mesquita, B., Key, T. J., de Hoogh, K., Concin, H., Nagel, G., Vilier, A., Grioni, S., Krogh, V., Tsai, M.-Y., Ricceri, F., Sacerdote, C., Galassi, C., Migliore, E., Ranzi, A., Cesaroni, G., Badaloni, C., Forastiere, F., Tamayo,  
875 I., Amiano, P., Dorronsoro, M., Trichopoulou, A., Bamia, C., Vineis, P., and Hoek, G.: Air pollution and lung cancer incidence in 17 European cohorts: prospective analyses from the European Study of Cohorts for Air Pollution Effects (ESCAPE), *The Lancet Oncology*, 14, 813–822, doi:10.1016/S1470-2045(13)70279-1, [http://www.thelancet.com/journals/lanonc/article/PIIS1470-2045\(13\)70279-1/abstract](http://www.thelancet.com/journals/lanonc/article/PIIS1470-2045(13)70279-1/abstract), 2013.
- Ren, X., Harder, H., Martinez, M., Leshner, R. L., Oligier, A., Simpas, J. B., Brune, W. H., Schwab, J. J.,  
880 Demerjian, K. L., He, Y., Zhou, X., and Gao, H.: OH and HO<sub>2</sub> Chemistry in the urban atmosphere of New York City, *Atmospheric Environment*, 37, 3639–3651, doi:10.1016/S1352-2310(03)00459-X, <http://www.sciencedirect.com/science/article/pii/S135223100300459X>, 2003.
- Rood, A. S.: Performance evaluation of AERMOD, CALPUFF, and legacy air dispersion models using the Winter Validation Tracer Study dataset, *Atmospheric Environment*, 89,  
885 707–720, doi:10.1016/j.atmosenv.2014.02.054, <http://www.sciencedirect.com/science/article/pii/S1352231014001502>, 2014.
- Soulhac, L., Salizzoni, P., Cierco, F. X., and Perkins, R.: The model SIRANE for atmospheric urban pollutant dispersion; part I, presentation of the model, *Atmospheric Environment*, 45, 7379–7395, doi:10.1016/j.atmosenv.2011.07.008, <http://www.sciencedirect.com/science/article/pii/S1352231011007096>,  
890 2011.
- Soulhac, L., Salizzoni, P., Mejean, P., Didier, D., and Rios, I.: The model SIRANE for atmospheric urban pollutant dispersion; PART II, validation of the model on a real case study, *Atmospheric Environment*, 49, 320–337, doi:10.1016/j.atmosenv.2011.11.031, <http://www.sciencedirect.com/science/article/pii/S1352231011012143>, 2012.



- 895 Steinbacher, M., Zellweger, C., Schwarzenbach, B., Bugmann, S., Buchmann, B., Ordóñez, C., Prevot, A. S. H., and Hueglin, C.: Nitrogen oxide measurements at rural sites in Switzerland: Bias of conventional measurement techniques, *J. Geophys. Res.*, 112, D11 307, doi:10.1029/2006JD007971, <http://onlinelibrary.wiley.com/doi/10.1029/2006JD007971/abstract>, 2007.
- Stocker, J., Hood, C., Carruthers, D., and McHugh, C.: ADMS-Urban: developments in modelling dispersion from the city scale to the local scale, *International Journal of Environment and Pollution*, 50, 308, 900 doi:10.1504/IJEP.2012.051202, <http://www.inderscience.com/link.php?id=51202>, 2012.
- Terrenoire, E., Bessagnet, B., Rouil, L., Tognet, F., Pirovano, G., Létinois, L., Beauchamp, M., Colette, A., Thunis, P., Amann, M., and Menut, L.: High-resolution air quality simulation over Europe with the chemistry transport model CHIMERE, *Geosci. Model Dev.*, 8, 21–42, doi:10.5194/gmd-8-21-2015, <http://www.geosci-model-dev.net/8/21/2015/>, 2015. 905
- Thunis, P., Pederzoli, A., and Pernigotti, D.: Performance criteria to evaluate air quality modeling applications, *Atmospheric Environment*, 59, 476–482, doi:10.1016/j.atmosenv.2012.05.043, <http://www.sciencedirect.com/science/article/pii/S1352231012005158>, 2012.
- U.S. Environment Protection Agency: Meteorological monitoring guidance for regulatory modeling applications, Tech. Rep. EPA-454/R-99-005, U.S. Environmental Protection Agency, Office of Air and Radiation, Office of Air Quality Planning and Standards, Research Triangle Park, N.C., 2000. 910
- Van Roosbroeck, S., Wichmann, J., Janssen, N. A. H., Hoek, G., van Wijnen, J. H., Lebet, E., and Brunekreef, B.: Long-term personal exposure to traffic-related air pollution among school children, a validation study, *Science of The Total Environment*, 368, 565–573, doi:10.1016/j.scitotenv.2006.03.034, <http://www.sciencedirect.com/science/article/pii/S004896970600266X>, 2006. 915
- Vardoulakis, S., Gonzalez-Flesca, N., and Fisher, B. E. A.: Assessment of traffic-related air pollution in two street canyons in Paris: implications for exposure studies, *Atmospheric Environment*, 36, 1025–1039, doi:10.1016/S1352-2310(01)00288-6, <http://www.sciencedirect.com/science/article/pii/S1352231001002886>, 2002.